

# From the middle stratosphere to the surface, using nitrous oxide to constrain the stratosphere-troposphere exchange of ozone

Daniel J. Ruiz<sup>1</sup> and Michael J. Prather<sup>1</sup>

<sup>1</sup>Department of Earth System Science, University of California, Irvine, CA 92697-3100, USA

*Correspondence to:* Daniel J. Ruiz (djruiz@uci.edu)

## Abstract

Stratosphere-troposphere exchange (STE) is an important source of tropospheric ozone, affecting all of atmospheric chemistry, climate, and air quality. The study of impacts needs STE fluxes to be resolved by latitude and month, and for this we rely on global chemistry models, whose results diverge greatly. Overall, we lack guidance from model-measurement metrics that inform us about processes and patterns related to the STE flux of ozone (O<sub>3</sub>). In this work, we use modeled tracers (N<sub>2</sub>O, CFCl<sub>3</sub>) whose distributions and budgets can be constrained by satellite and surface observations, allowing us to follow stratospheric signals across the tropopause. The satellite derived photochemical loss of N<sub>2</sub>O on annual and quasi-biennial cycles can be matched by the models. The STE flux of N<sub>2</sub>O-depleted air in our chemistry transport model drives surface variability that closely matches observed fluctuations on both annual and quasi-biennial cycles, confirming the modeled flux. The observed tracer correlations between N<sub>2</sub>O and O<sub>3</sub> in the lowermost stratosphere provide a hemispheric scaling of the N<sub>2</sub>O STE flux to that of O<sub>3</sub>. For N<sub>2</sub>O and CFCl<sub>3</sub>, we model greater southern hemispheric STE fluxes, a result supported by some metrics, but counter to prevailing theory of wave-driven stratospheric circulation. The STE flux of O<sub>3</sub>, however, is predominantly northern hemispheric, but evidence shows that this is caused by the Antarctic ozone hole reducing southern hemispheric O<sub>3</sub> STE by 14%. Our best estimate of the current STE O<sub>3</sub> flux based on a range of constraints is 400 Tg(O<sub>3</sub>)/yr with a one-sigma uncertainty of ±15% and with a NH:SH ratio ranging from 50:50 to 60:40. We identify a range of observational metrics that can better constrain the modeled STE O<sub>3</sub> flux in future assessments.

## 1. Introduction & Background

The influx of stratospheric ozone (O<sub>3</sub>) into the troposphere affects its distribution, variability, lifetime, and thus its role in driving climate change and surface air pollution (Zeng et al., 2010; Hess et al., 2015; Williams et al., 2019). The net stratosphere-to-troposphere exchange (STE) flux of O<sub>3</sub> has a regular seasonal cycle in each hemisphere that is an important part of the tropospheric O<sub>3</sub> budget (Stohl et al., 2003). Such fluxes are not directly observable, and we rely on observational estimates using trace-gas ratios, in particular the O<sub>3</sub>:N<sub>2</sub>O ratio in the lower stratosphere (Murphy and Fahey, 1994; McLinden et al., 2000), or dynamical calculations using measured/modeled winds and O<sub>3</sub> abundances (Gettelman et al., 1997; Olsen et al., 2004; Yang et al., 2016). The uncertainty in these estimates does not effectively constrain the wide range found in the models being used to project future ozone (Young et al., 2013, 2018; Griffiths et al., 2021). Here we present the case for using the observed variations in nitrous oxide (N<sub>2</sub>O) from the middle stratosphere to the surface in order to constrain the STE flux of O<sub>3</sub>. A similar case

47 has been made for the radionuclide  $^7\text{Be}$  (Liu et al., 2016), but  $\text{N}_2\text{O}$  has a wealth of model-  
48 observation metrics on hemispheric, seasonal, and interannual scales that constrains its STE flux  
49 very well (Prather et al., 2015; Ruiz et al., 2021).

50  
51 Ozone-rich stratospheric air has been photochemically aged and is depleted in trace gases such as  
52  $\text{N}_2\text{O}$  and chlorofluorocarbons (CFCs). For these trace gases, the overall circulation from  
53 tropospheric sources to stratospheric destruction and back is part of the lifecycle that maintains  
54 their global abundance (Holton, 1990). For  $\text{N}_2\text{O}$  and CFCs, this cycle of (i) loss in the middle to  
55 upper stratosphere, (ii) transport to the lowermost stratosphere (Holton et al., 1995), and then (iii)  
56 influx into the troposphere produces surface variations not related to surface emissions  
57 (Hamilton and Fan, 2000; Nevison et al., 2004; Hirsch et al., 2006; Montzka et al., 2018; Ray et  
58 al., 2020; Ruiz et al., 2021). In this work we relate our modeled STE fluxes to variations at the  
59 surface and throughout the stratosphere, linking the fluxes of  $\text{N}_2\text{O}$  to  $\text{O}_3$  through stratospheric  
60 measurements. Our goal is to develop a set of model metrics founded on observations that are  
61 related to the STE  $\text{O}_3$  flux and can be used with an ensemble of models to determine a better,  
62 constrained estimate for the flux, including seasonal, interannual, and hemispheric patterns. This  
63 approach is similar to efforts involving the ozone depletion recovery time (Strahan et al.,  
64 2011) and projections of future warming (Liang et al., 2020; Tokarska et al., 2020).

65  
66 In a previous work (Ruiz et al., 2021, hence R2021) we showed that historical simulations with  
67 three chemistry transport models (CTMs) were able to match the interannual surface variations  
68 observed in  $\text{N}_2\text{O}$ . These were clearly driven by the stratospheric quasi-biennial oscillation  
69 (QBO) which appears to be the major interannual signal in stratospheric circulation and STE  
70 (Kinnersley and Tung, 1999; Baldwin et al., 2001; Olsen et al., 2019). In this work, we calculate  
71 the monthly latitudinal STE fluxes of  $\text{O}_3$ ,  $\text{N}_2\text{O}$ , and  $\text{CFCl}_3$  (F11), establish a coherent picture  
72 relating fluxes to observed abundances, and summarize the methods in Section 2. In section 3,  
73 we examine the annual and interannual cycles as well as geographic patterns of modeled STE  
74 flux. In section 4, we relate the surface variability of  $\text{N}_2\text{O}$  to its STE flux. We find some  
75 evidence to support our model result that the STE flux of depleted- $\text{N}_2\text{O}$  air is greater in the  
76 southern hemisphere than in the northern, thus altering the asymmetry in surface emissions in the  
77 source inversions (Nevison et al., 2007; Thompson et al., 2014). In section 5, we examine the  
78 lowermost stratosphere to understand the large north-south asymmetry found in  $\text{O}_3$  STE versus  
79  $\text{N}_2\text{O}$  or F11 STE, and find a clear signal of the Antarctic ozone hole in STE. In section 6, we  
80 examine the consistency of the model calculations of STE flux and derive a best estimate for the  
81  $\text{O}_3$  flux from this and previous studies. We summarize a sequence of model metrics, primarily  
82 using  $\text{O}_3$  and  $\text{N}_2\text{O}$ , that can narrow the range in the tropospheric  $\text{O}_3$  budget terms for the multi-  
83 model intercomparison projects used in tropospheric chemistry and climate assessments.

## 84 85 **2. Methods**

86  
87 The modeled STE fluxes here are calculated with the UCI (University of California Irvine) CTM  
88 driven by 3-hour forecast fields from the European Centre for Medium-range Weather Forecasts  
89 (ECMWF) Integrated Forecast System (IFS Cycle 38r1 T159L60) for years 1990-2017, as are  
90 the calculations in R2021. The CTM uses the IFS native 160x320 Gauss grid ( $\sim 1.1^\circ$ ) with 60  
91 layers, about 35 of which are in the troposphere. The stratospheric chemistry uses the linearized  
92 model Linoz v3 and includes  $\text{O}_3$ ,  $\text{N}_2\text{O}$ ,  $\text{NO}_y$ ,  $\text{CH}_4$ , and F11 as transported trace gases (Hsu and

93 Prather, 2010; Prather et al., 2015; Ruiz et al., 2021). There is no tropospheric chemistry, but  
94 rather a boundary-layer e-fold to a specified abundance, or a surface boundary reset to an  
95 abundance. Equivalent effective stratospheric chlorine levels are high enough to drive an  
96 Antarctic ozone hole, which is observed throughout this period. Thus, the ozone-hole chemistry  
97 in Linoz v3 is activated for all years, and the amount of O<sub>3</sub> depleted depends on the Antarctic  
98 meteorology of that year (Hsu and Prather, 2010).

99  
100 The STE flux is calculated using the e90 definition of tropospheric grid cells (Prather et al.,  
101 2011) and the change in tropospheric tracer mass from before to after each tracer transport step  
102 as developed at UCI (Hsu et al., 2005; Hsu and Prather, 2009; Hsu and Prather, 2014). This  
103 method is precise and geographically accurate for O<sub>3</sub> and is self-consistent with a CTM's tracer-  
104 transport calculation (Tang et al., 2013; Hsu and Prather, 2014). Extensive comparisons with  
105 other methods of calculating STE are shown in Hsu and Prather (2014). Annual-mean STE  
106 fluxes are calculated from the full 28-year (336 month) time series as 12-month running means,  
107 and the annual cycle of monthly fluxes is the average of the 28 values for each month.

108  
109 R2021 modeled the surface signal of stratospheric loss with the decaying tracers, N2OX and  
110 F11X (e.g., (Hamilton and Fan, 2000; Hirsch et al., 2006). These X-tracers have the identical  
111 stratospheric chemical loss frequencies as N<sub>2</sub>O and CFC<sub>3</sub>, respectively, but no surface sources  
112 and are therefore affected only by the stratospheric sink and atmospheric transport. The multi-  
113 decade (F11X) to century (N2OX) decays are easily rescaled using a 12-month smoothing filter  
114 to give stationary results and a tropospheric mean abundance of 320 ppb. We treat F11X like  
115 N2OX with the same initial conditions and molecular weight. Budgets for N2OX are reported,  
116 as in N<sub>2</sub>O studies (Tian et al., 2020), as Tg of N as N<sub>2</sub>O. These rescaled N2OX and F11X tracers  
117 are designated simply as N2O (not N<sub>2</sub>O) and F11. Our F11 STE fluxes are thus unrealistically  
118 large compared to current CFC<sub>3</sub> fluxes, but can be easily compared with our N2O results.

119  
120 When trying to calculate the STE flux of N<sub>2</sub>O-depleted air across the tropopause, we found that  
121 the Hsu method was numerically noisy because the gradient across the tropopause, unlike that of  
122 O<sub>3</sub>, was negligible. Thus, for this work we created the complementary tracers cN2OX and  
123 cF11X: for each kg of the X-tracer (i.e., N2OX) destroyed by photochemistry, 1 kg of its  
124 complementary tracer (cN2OX) is created. Air parcels that are depleted in N2OX (F11X) are  
125 therefore rich in cN2OX (cF11X). After crossing the tropopause, cN2OX and cF11X are  
126 removed through rapid uptake in the boundary layer, thus creating sharp gradients at the  
127 tropopause in parallel with that of O<sub>3</sub>. As a check, we compared the boundary layer sinks of the  
128 c-tracers with their e90-derived STE fluxes and find that their sums are identical. The c-tracers  
129 and their STE fluxes are rescaled as are the X-tracers to give them a stationary time series  
130 corresponding to a tropospheric abundance of 320 ppb for their parallel X tracers. We designate  
131 these scaled tracers simply as cN2O and cF11.

### 132 133 **3. Modeled STE fluxes**

#### 134 135 *3.1 Global and hemispheric means*

136  
137 The 28-year mean of global O<sub>3</sub> STE is 390±16 Tg/yr (positive flux means stratosphere to  
138 troposphere, the ± values are the standard deviation of the 28 annual means and do not represent

139 uncertainty). This value is well within the uncertainty in the observation-based estimates  
140 (Murphy and Fahey, 1994; Olsen et al., 2001), and far from the extreme ranges of the 34 models  
141 in the latest Tropospheric Ozone Assessment Report (Young et al., 2018), 150 to 940 Tg/yr. The  
142 global STE flux of cN<sub>2</sub>O is 11.5±0.7 Tg/yr, and that of cF11 is 23.5±1.5 Tg/yr. These fluxes for  
143 cN<sub>2</sub>O and cF11 match the total long-term troposphere-to-stratosphere flux of N<sub>2</sub>O and F11 as  
144 derived from their stratospheric losses. The cF11 budget is about twice as large as cN<sub>2</sub>O,  
145 because F11 is photolyzed rapidly in the lower-middle stratosphere (~24 km) instead of the  
146 upper stratosphere like N<sub>2</sub>O (~32 km). The seasonal mean pattern of STE fluxes are shown in  
147 Figure 1. The large majority of STE flux enters the troposphere at 25°-45° latitude in each  
148 hemisphere, but there is a broadening of the northern flux to 65°N in Jun-Jul. The importance of  
149 this region about the sub-tropical jet for STE is supported by satellite data where stratospheric  
150 folding events (high O<sub>3</sub> in the upper troposphere) are found at the bends of the jet (Tang and  
151 Prather, 2010).

152  
153 Given the small STE fluxes in the core tropics, the northern hemisphere (NH) and southern  
154 hemisphere (SH) fluxes are distinct. The annual mean of NH O<sub>3</sub> STE is 208±11 Tg/yr and is  
155 slightly larger than the SH mean of 182±11 Tg/yr. This NH:SH ratio of 53:47 is typically found  
156 in other studies (Gettelman et al., 1997; Hsu and Prather, 2009; Yang et al., 2016), although  
157 some have higher ratios like 58:42 (Hegglin and Shepherd, 2009; Meul et al., 2018). In contrast,  
158 for cN<sub>2</sub>O and cF11, the NH flux (5.1±0.4 Tg/yr and 10.6±0.8 Tg/yr, respectively) is smaller than  
159 the SH flux (6.4±0.5 Tg/yr and 12.9±1.0 Tg/yr, respectively), giving a NH:SH ratio of about  
160 45:55. The established view on STE is that the flux is wave-driven and under downward control,  
161 and thus the NH flux is much greater than the SH flux (see Table 1 of Holton et al., 1995; also  
162 Appenzeller et al., 1996). Our unexpected results require further analysis including evidence for  
163 hemispheric asymmetry in observations which is shown in section 4 along with other model  
164 metrics.

165  
166  
167  
168  
169  
170  
171  
172

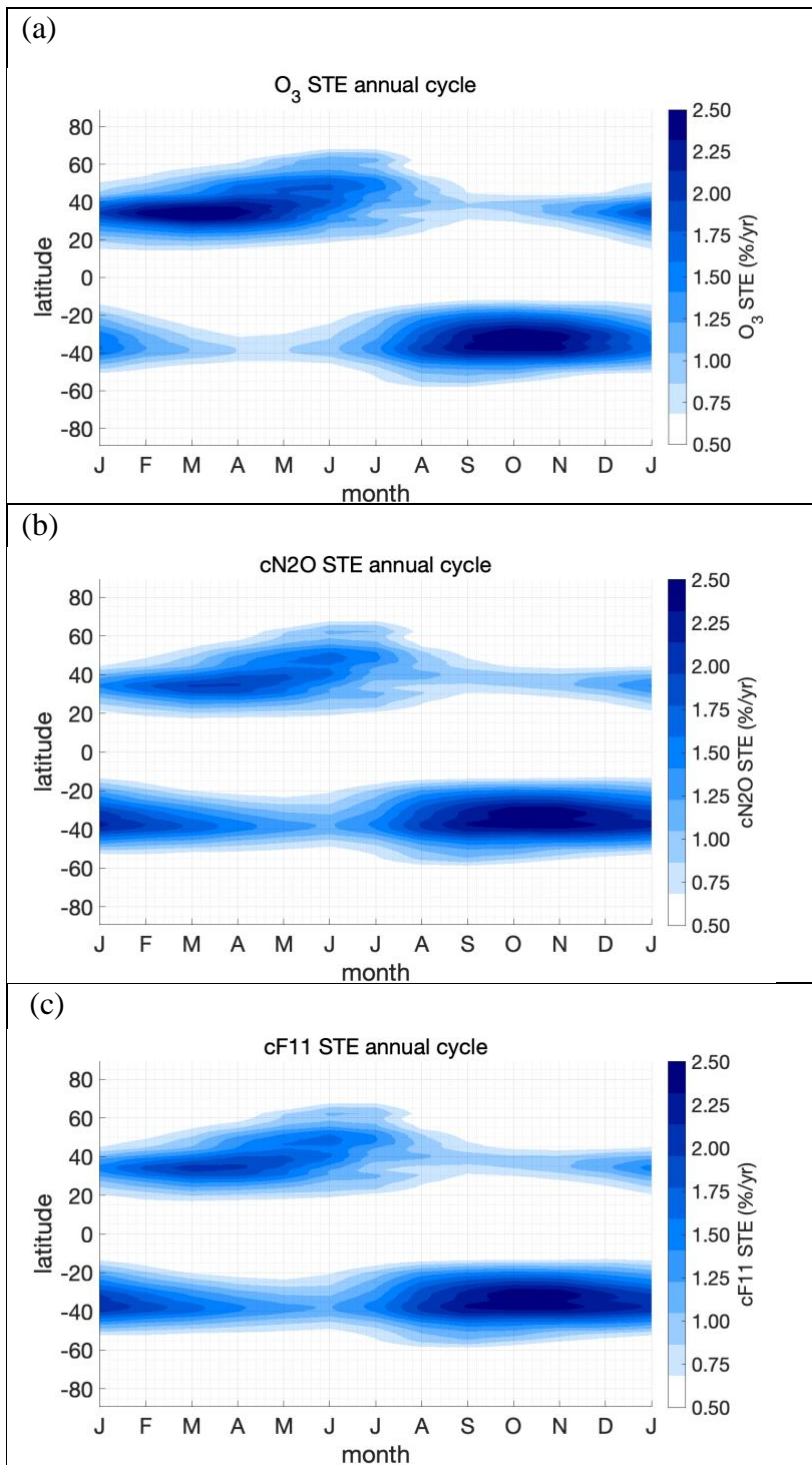


**Figure 1.** The seasonal (latitude by month) cycle of STE flux (Tg/yr) for (a)  $O_3$ , (b) cN<sub>2</sub>O, and (c) cF11. Each month is averaged for years 1990-2017 (e.g., the 28 Januarys are averaged). The colorbar units are % of global, annual mean STE in each bin (1 month by  $\sim 1.1^\circ$  latitude).

173  
174

### 175 3.2 Seasonal cycle

176

177 The seasonal cycles of STE fluxes summed over global, NH, and SH are shown in Figure 2. The  
178 scales are given as the annual rate (as if the monthly rate were maintained for the year), and each  
179 species has a different axis. The right y-axes are kept at a N<sub>2</sub>O:F11 ratio of 1:2. Despite large  
180 differences in the stratospheric chemistry across all three species, the seasonal cycle of STE is  
181 highly correlated (Pearson's correlation coefficient  $cc > 0.98$ , except for SH O<sub>3</sub>), indicating that  
182 all three enter the troposphere from a seasonally near-uniform mixture of O<sub>3</sub>:N<sub>2</sub>O:F11 in the  
183 lowermost stratosphere.

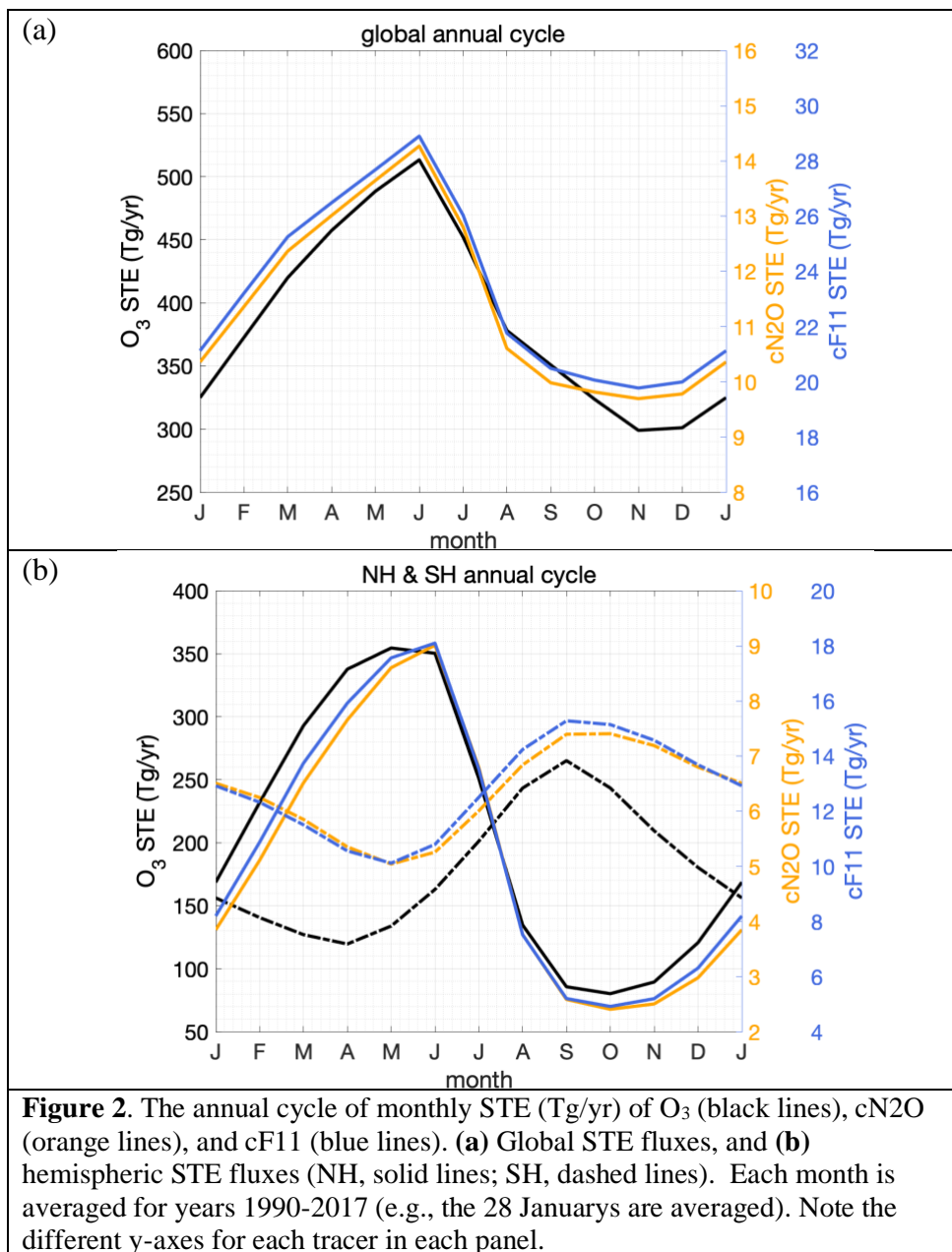
184

185 Global STE peaks in June and reaches a minimum in November. The two hemispheres have  
186 dramatically different seasonal amplitudes and somewhat opposite phases. NH peak STE for all  
187 3 species occurs in the late boreal spring (May-June), while that in the SH occurs at the start of  
188 austral spring (September-October). In the NH O<sub>3</sub> STE peaks a month before the c-tracers, and  
189 in the SH the whole annual cycle of O<sub>3</sub> is shifted a month earlier. The NH STE seasonal  
190 amplitude is very large for all species (~ 4:1 ratio max-to-min) with exchange almost ceasing in  
191 the fall. In contrast, the SH STE is more uniform year-round with a 1.5:1 ratio for cN<sub>2</sub>O and  
192 cF11, and 2.2:1 for O<sub>3</sub>. Other models with similar NH and SH O<sub>3</sub> fluxes show different seasonal  
193 amplitudes and phasing (see Fig. 6 of Tang et al., 2021), which will affect tropospheric O<sub>3</sub>  
194 abundances. It is important to develop observational metrics that test the seasonality of the  
195 lowermost stratosphere related to STE fluxes, and to establish monthly STE fluxes as a standard  
196 model diagnostic.

197

198 An interesting result here is the very tight correlation of the monthly cN<sub>2</sub>O and cF11 STE while  
199 the O<sub>3</sub> STE is sometimes shifted. Loss of N<sub>2</sub>O and F11 occurs at very different altitudes in the  
200 tropical stratosphere (~32 km and ~24 km, respectively), but both have similar seasonality in  
201 loss, driven mostly by the intensity of sunlight along the Earth's orbit (N<sub>2</sub>O loss peaks in Feb and  
202 reaches a minimum in July, see Fig. 4 from Prather et al. (2015). Photochemical losses of N<sub>2</sub>O  
203 and F11 drop quickly for air descending from the altitudes of peak loss in the tropics and hence  
204 the relative cN<sub>2</sub>O and cF11 STE fluxes are locked in. O<sub>3</sub>, however, continues to evolve  
205 photochemically from 24 km to 16 km (upper boundary of the lowermost stratosphere), through  
206 net photochemical production in the tropics and loss at mid- and high-latitudes that depends on  
207 sunlight and is thus seasonal. There may be observational evidence for the patterns modeled  
208 here in the correlation of these three tracers in the lower (16-20 km) and lowermost (12-16 km)  
209 extratropical stratosphere (see section 4).

210



211  
 212  
 213  
 214  
 215  
 216  
 217  
 218  
 219  
 220  
 221

### 3.3 Interannual variability

Interannual variability (IAV) of N<sub>2</sub>O loss and its lifetime is associated primarily with the QBO (most recently, R2021). When the QBO is in its easterly (westerly) phase the entire overturning circulation is enhanced (suppressed) (Baldwin et al., 2001). This results in more (less) air rich in N<sub>2</sub>O and F11 being transported from the troposphere to the lower or middle stratosphere, thereby increasing (decreasing) the N<sub>2</sub>O and F11 sinks (Prather et al., 2015; Strahan et al., 2015). From the tropical stratosphere, the overturning circulation transports air depleted in N<sub>2</sub>O and F11 into the lowermost extratropical stratosphere, where it enters the troposphere. R2021 showed that the

222 observed surface variability of N<sub>2</sub>O from this circulation can be modeled and has a clear QBO  
223 signal, but one that is not strongly correlated with the QBO signal in stratospheric loss.  
224

225 We generate the IAV of STE fluxes for O<sub>3</sub>, cN<sub>2</sub>O, and cF11 in Figure 3abc with panels for  
226 global, NH, and SH. Values are 12-month running means, and so the first modeled point at  
227 1990.5 is the sum of STE for Jan through Dec of 1990. In Figures 3bc, we also show the  
228 seasonal amplitude of STE with double-headed arrows on the left (O<sub>3</sub>) and right (cN<sub>2</sub>O and  
229 cF11). In a surprising result, the large NH-SH differences in seasonal amplitude are not reflected  
230 in the IAV where NH and SH amplitudes are similar for all three tracers. The QBO modulation  
231 of the lowermost stratosphere and STE appears to be unrelated to the seasonal cycle in STE.  
232

233 Global STE for all three tracers shows QBO-like cycling throughout the 1990-2017 time series:  
234 cN<sub>2</sub>O and cF11 are well correlated ( $cc \sim 0.9$ ), but either species with O<sub>3</sub> is much less so ( $cc <$   
235  $0.7$ ). The hemispheric breakdown provides key information regarding O<sub>3</sub>. In the NH the STE  
236 IAV is similar across all three tracers with high correlation coefficients ( $cc = 0.82$  for O<sub>3</sub>-cN<sub>2</sub>O,  
237  $0.83$  for O<sub>3</sub>-cF11, and  $0.94$  for cN<sub>2</sub>O-cF11). Conversely in the SH, O<sub>3</sub> STE diverges from the c-  
238 tracer fluxes, showing opposite-sign peaks in 2003 and 2016. The corresponding SH  
239 correlations are ( $cc = 0.38, 0.65, 0.85$ ). The loss of correlation between cN<sub>2</sub>O and cF11 is  
240 unusual: cN<sub>2</sub>O STE drifts downward relative to cF11 STE, particularly after 2007; nevertheless,  
241 the fine structure after 2007 is well matched in both tracers.  
242

243 In the SH, the massive loss of O<sub>3</sub> within the Antarctic vortex, when mixed with the extra-polar  
244 lowermost stratosphere will systematically shift the O<sub>3</sub> STE to lower values, with less impact on  
245 the cN<sub>2</sub>O and cF11 STE. The IAV of the Antarctic winter vortex, in terms of the amount of O<sub>3</sub>  
246 that is depleted (see Fig. 4-4 of WMO, 2018), appears to drive the decorrelation of the SH STE  
247 fluxes and is analyzed in section 4.  
248

249 In the NH, the high variability of the Arctic winter stratosphere can modulate the total O<sub>3</sub> STE  
250 flux (e.g., Hsu and Prather, 2009) but appears to maintain the same relative ratio with the cN<sub>2</sub>O  
251 and cF11 fluxes. Model results here indicate that in the NH, the IAV of O<sub>3</sub>, cN<sub>2</sub>O, and cF11 STE  
252 fluxes are synchronized, and thus the air masses entering the lowermost stratosphere have the  
253 same chemical mixtures from year to year. We know that cold-temperature activation of  
254 halogen-driven O<sub>3</sub> depletion in the Arctic winter at altitudes above 400 K (potential temperature)  
255 can produce large IAV in column ozone (Manney et al., 2011); but the magnitude is still much  
256 smaller than in the Antarctic; and it may not reach into the lowermost stratosphere (<380K  
257 potential temperature). This model accurately simulates Antarctic O<sub>3</sub> loss (section 4), but we  
258 have not evaluated it for Arctic loss, and the Arctic conditions operate closer to the thresholds  
259 initiating loss where Linoz v3 chemistry may be inadequate. The same meteorology and  
260 transport model with full stratospheric chemistry is able to simulate Arctic O<sub>3</sub> loss (Oslo's  
261 CTM2: Isaksen et al., 2012), and thus it will be possible to re-evaluate the NH IAV with such  
262 models or with lowermost stratosphere tracer measurements.  
263  
264  
265  
266  
267



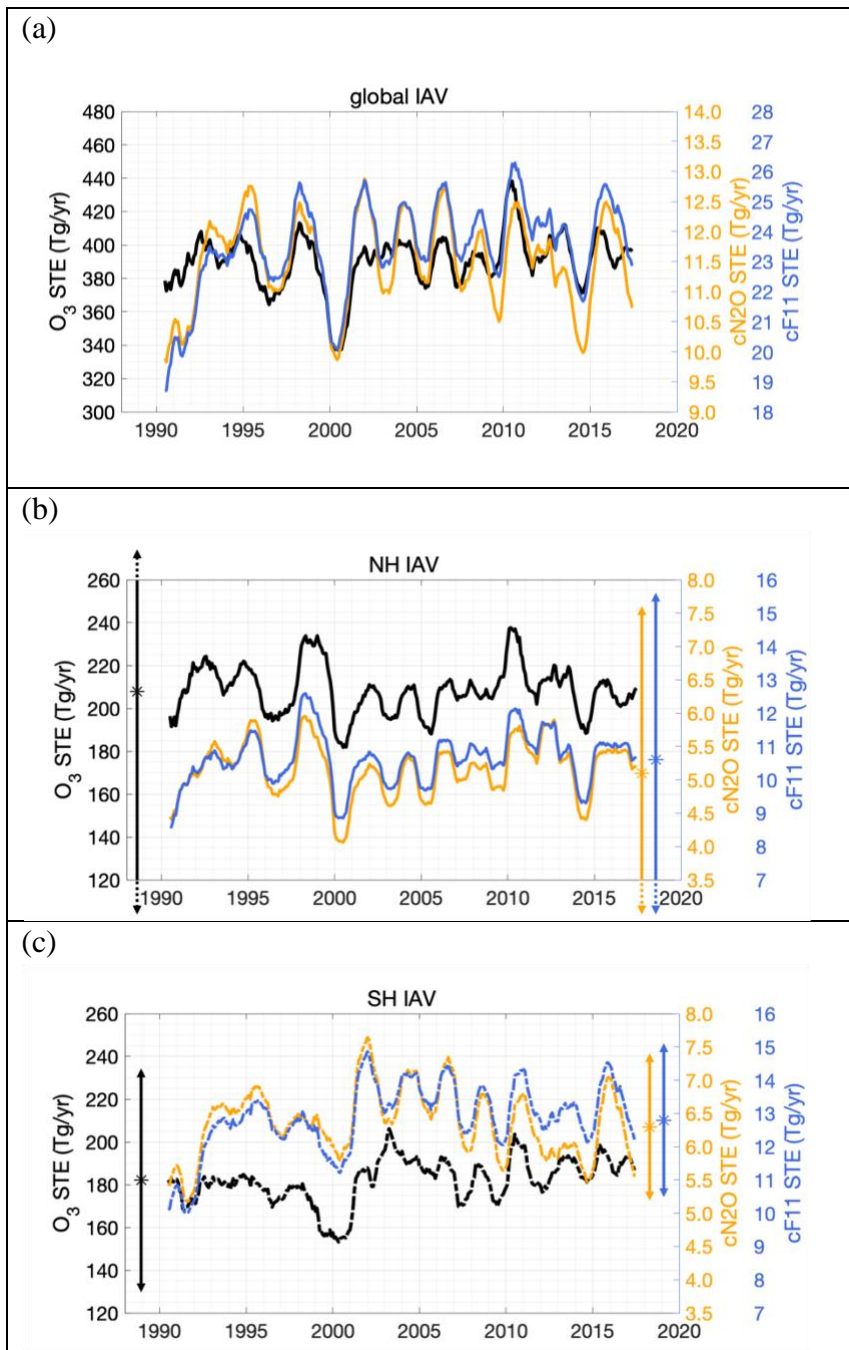


**Figure 3.** (a) Global STE (Tg/yr), calculated at e90 tropopause, of O<sub>3</sub> (black line; left y-axis), cN<sub>2</sub>O (orange line; orange right y-axis), and cF11 (blue line; blue right y-axis) for years 1990-2017. Values are 12-month running means, and so the first point at 1990.5 is the sum of STE for Jan through Dec of 1990. (b) NH STE. (c) SH STE. The scales for cN<sub>2</sub>O and cF11 are kept in a 1:2 ratio. The asterisks and vertical double-headed arrows (b & c) depict the seasonal mean and amplitude for each species in each hemisphere.

268  
269

270 **3.4 The link from stratospheric loss to STE flux**

271  
272 What is unusual about the very tight correlation of cN<sub>2</sub>O and cF11 STE fluxes is that the  
273 photochemical loss of N<sub>2</sub>O and F11 occurs at very different altitudes in the tropical stratosphere,  
274 which are not in phase with respect to the QBO as shown in R2021 (their Fig. 2). The separate  
275 phasing of cN<sub>2</sub>O and cF11 production is lost, presumably by diffusive tracer transport, by the  
276 time they reach the extratropical lowermost stratosphere. The overall synchronization of the  
277 STE fluxes implies that the absolute STE flux is driven primarily by variations in venting of the  
278 lowermost stratosphere as expected (Holton et al., 1995; Appenzeller et al., 1996) rather than by  
279 variations in the chemistry of the middle stratosphere.

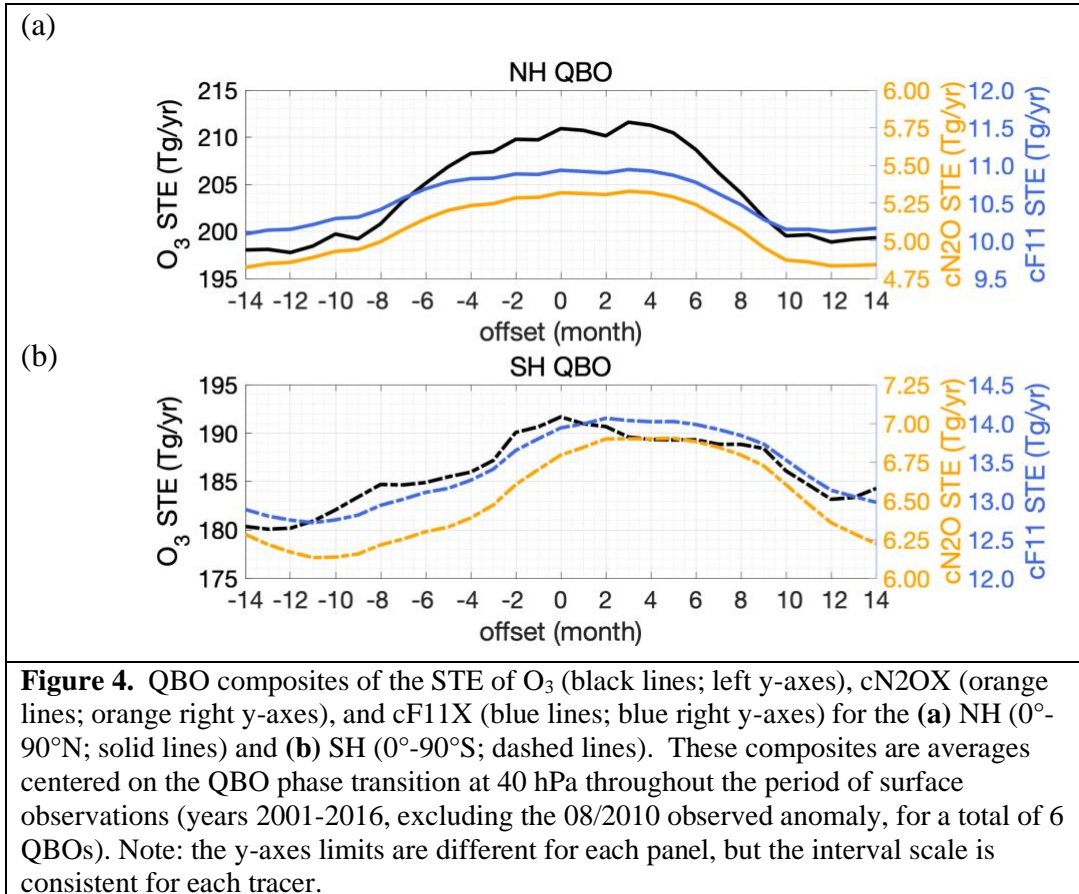
280  
281 This disconnect between the chemical signals generated by the prominent QBO signature of  
282 wind reversals, upwelling in the tropical stratosphere, and the STE fluxes is also clear in the  
283 magnitude of the loss versus STE. For N<sub>2</sub>O, the IAV of cN<sub>2</sub>O production has a range of  $\pm 0.5$   
284 Tg/yr, whether from the Aura Microwave Limb Sounder (Aura-MLS) observations or the model;  
285 whereas the IAV of cN<sub>2</sub>O STE flux is  $\pm 1.1$  Tg/yr. The same is true in relative terms for cF11.  
286 Thus, the modulation of the lowermost stratosphere by the QBO is clearly a part of the overall  
287 changes in stratospheric circulation related to the QBO (Tung and Yang, 1994a; Kinnersley and  
288 Tung, 1999) and is the dominant source of IAV for these three greenhouse gases.

289  
290 **3.5. The QBO signal**

291  
292 To examine the QBO cycle in STE flux, we build a composite pattern (see R2021, Fig. 3 of N<sub>2</sub>O  
293 surface variations), by synchronizing the STE IAV in Figure 2 with the QBO cycle. The sync  
294 point (offset = 0 months) is taken from one of the standard definitions of the QBO phase change,  
295 i.e., the shift in sign of the 40-hPa tropical zonal wind from easterly to westerly (Newman,  
296 2020). The 1990-2017 model period has 12 QBO cycles, but we restrict our analysis here to  
297 years 2001-2016 to overlap with the observed surface N<sub>2</sub>O data. This period includes seven  
298 QBO phase transitions (01/2002, 03/2004, 04/2006, 04/2008, 08/2010, 04/2013, 07/2015), but  
299 the observed surface N<sub>2</sub>O is highly anomalous during the QBO centered on 08/2010 (R2021), so  
300 we remove it from our comparison for consistency with R2021 (see their Fig S4d). The resulting  
301 QBO composites for NH and SH in Figure 4 span 28 months.

302  
303 In the NH, the QBO modulation of all three tracers is similar: STE flux begins to increase at an  
304 offset of -8 months and continues to increase slowly for a year, peaking at an offset of +4  
305 months; thereafter it decreases more rapidly in about ½ year (offset = +10). The rise-and-fall  
306 cycle takes about 18 months. In the SH, the pattern for cN<sub>2</sub>O and cF11 is more sinusoidal and is  
307 shifted later by ~3 months. The SH amplitude of the c-tracers is slightly larger relative to the  
308 hemispheric mean flux than in the NH, and thus the SH QBO signal is larger than the NH by  
309 about 40%. Thus, over the typical QBO cycle centered on the sync point, more depleted N<sub>2</sub>O  
310 and F11 is entering the SH than in the NH. For O<sub>3</sub>, the SH modulation of STE is irregular and  
311 reduced compared with the NH. Our hypothesis here, consistent with the annual cycle of STE  
312 (Figure 1), is that the breakup of the Antarctic ozone hole has a major impact on STE,  
313 particularly that of O<sub>3</sub>, and that its signal has large IAV that does not synchronize with the QBO.  
314 Surprisingly, the large wintertime IAV in the NH Arctic, in the form of sudden stratospheric  
315 warmings, does not seem to have a major role in STE fluxes as noted above. This model may

316 miss some of the Arctic O<sub>3</sub> depletion, but it accurately simulates the warmings, which must have  
 317 a small impact on STE because they do not disrupt the clear QBO signal in the c-tracers.  
 318



319  
 320  
 321 **4. Surface variability of N<sub>2</sub>O related to STE flux**  
 322  
 323 Surface variability of N<sub>2</sub>O is driven by surface emissions, stratospheric loss, and atmospheric  
 324 transport that mixes the first two signals. R2021 explored the variability originating only from  
 325 stratospheric chemistry using the decaying tracer N2OX. Here, we use surf-N2O to denote the  
 326 surface abundances of N2OX when corrected to steady state. R2021 showed that three  
 327 independent chemistry-transport models produced annual and QBO patterns in surface N<sub>2</sub>O  
 328 simply from stratospheric loss. In this paper we link surf-N2O to the STE cN2O flux, which is  
 329 linked above to the STE O<sub>3</sub> flux.

330  
 331 The observed surface N<sub>2</sub>O, denoted obs-N<sub>2</sub>O and taken from the NOAA network (Dlugokencky  
 332 et al., 2019), shows a slowly increasing abundance (~0.9 ppb/yr) with a clear signal of annual  
 333 and interannual variability at some latitudes (see R2021). We calculate annual and QBO-  
 334 composite obs-N<sub>2</sub>O after de-trending and restrict analysis in this section to model years 2001-  
 335 2016 to be consistent with the surface data. The latitude-by-month pattern of obs-N<sub>2</sub>O includes  
 336 the impact of both stratospheric loss (~13.5 Tg/yr) and surface emissions (~17 TgN/yr), with the  
 337 preponderance of emissions being in the NH (Tian et al., 2020). Total emissions are not

338 expected to have large IAV but may have a seasonal cycle. The seasonal variation of surface  
339 N<sub>2</sub>O can also be driven by seasonality in the interhemispheric mixing of the NH-SH gradient (~1  
340 ppb).

341  
342

#### 343 *4.1 Annual cycle*

344

345 Figure 5 replots the hemispheric mean annual cycles of cN<sub>2</sub>O STE flux alongside the annual  
346 cycles of surf-N<sub>2</sub>O and obs-N<sub>2</sub>O. As noted above, the STE in each hemisphere is almost in  
347 opposite phase, as is the modeled surf-N<sub>2</sub>O (taken from Fig. 5 of R2021). The NH:SH  
348 amplitude ratio is about 2.4:1 for both STE and surf-N<sub>2</sub>O. The lag from peak STE flux of cN<sub>2</sub>O  
349 (negative N<sub>2</sub>O) to minimum surf-N<sub>2</sub>O is about 3 months. Such a 90° phase shift is expected for  
350 the seasonal variation of a long-lived tracer relative to a seasonal source or sink. The time lag  
351 between the signal at the tropopause and at the surface, the tropospheric turnover time, should be  
352 no more than a month. Surprisingly, the cN<sub>2</sub>O STE seasonal amplitude is much larger in the NH  
353 ( $\pm 3.4$  Tg/yr) than in the SH ( $\pm 1.3$  Tg/yr), although the SH mean (6.5 Tg/yr) is larger than the NH  
354 (5.2 Tg/yr). Essentially, there is more variability of air depleted in N<sub>2</sub>O entering the NH, but air  
355 entering the SH has a larger overall deficit. Thus in our model, the stratosphere creates a NH-SH  
356 gradient of +0.3 ppb at the surface, which is a significant fraction of the observed N-S difference  
357 of +1.3 ppb (R2021). This important result needs to be verified with other models or analyses  
358 because it constrains the NH-SH location of sources.

359

360 In the NH, as noted in R2021, the two surface abundances, surf-N<sub>2</sub>O and obs-N<sub>2</sub>O, have the  
361 same amplitude and phase, implying that, if the model is correct, the emissions-driven surface  
362 signal has no seasonality, although we know that some important emissions are seasonal  
363 (Butterbach-Bahl et al., 2013). In the SH, the surf-N<sub>2</sub>O signal is much smaller, in parallel with  
364 the small seasonal amplitude in cN<sub>2</sub>O STE, but it is out of phase with the obs-N<sub>2</sub>O. This result  
365 implies that the SH has some highly seasonal sources, or simply that the forcing of SH surf-N<sub>2</sub>O  
366 by the seasonal cycle of cN<sub>2</sub>O is weak. Indeed, this is what we might expect from Figure 3: In  
367 the NH the seasonal amplitude in N<sub>2</sub>O overwhelms the IAV amplitude and is driving the obs-  
368 N<sub>2</sub>O; but in the SH, both amplitudes are comparable. Given the quasi-regular nature of the  
369 QBO, it would interfere with the seasonal cycle and likely change its phase (as found for other  
370 models in R2021).

371

372 In the NH, the annual cycle of O<sub>3</sub> and cN<sub>2</sub>O STE are clearly linked. If we accept that the obs-  
373 N<sub>2</sub>O NH seasonal cycle is simply driven by the STE flux, then how will tropospheric O<sub>3</sub> respond  
374 seasonally? A mole-fraction scaling of the STE fluxes gives an O<sub>3</sub>:N<sub>2</sub>O ratio of ~25, and thus  
375 scaling the surf-N<sub>2</sub>O amplitude gives a large O<sub>3</sub> surface seasonality of ~18 ppb. However, the  
376 residence time of a tropospheric O<sub>3</sub> perturbation is ~1 month, and thus the peak surface  
377 abundance will lag the peak STE flux by only about a month and not by 3 months as for N<sub>2</sub>O.  
378 O<sub>3</sub> will equilibrate with the flux on monthly timescales and not accumulate. Thus, our estimate  
379 is that NH 30°-90° surface ozone might increase about 5 ppb, peaking in June, due to the STE  
380 flux. In the SH, seasonal patterns are weaker and not well defined, and thus no obvious STE O<sub>3</sub>  
381 signal is expected.

382

383

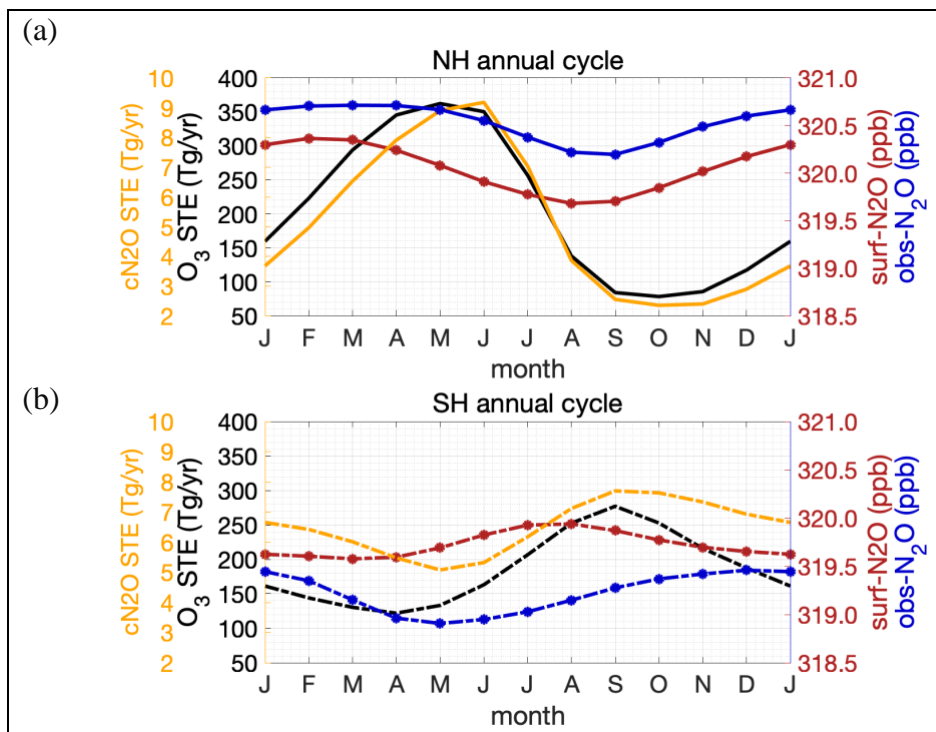


**Figure 5.** The annual cycle of O<sub>3</sub> and cN<sub>2</sub>O STE (black and orange lines; left y-axes), and the surf-N<sub>2</sub>O and obs-N<sub>2</sub>O (red and blue knotted lines; right y-axes) taken from R2021 (see their figure 5) for the (a) NH and (b) SH. cN<sub>2</sub>O, surf-N<sub>2</sub>O, and obs-N<sub>2</sub>O has been rescaled to reflect that of a tropospheric abundance of 320 ppb. The hemispheric domains for STE is defined as 0°-90° while the surf-N<sub>2</sub>O and obs-N<sub>2</sub>O is from 30°-90° N/S. Note: the left y-axis limits are different between the tracers, but the interval scale is the same.

384  
385  
386  
387  
388  
389  
390  
391  
392  
393  
394  
395  
396  
397  
398  
399  
400  
401  
402

#### 4.2. QBO cycle

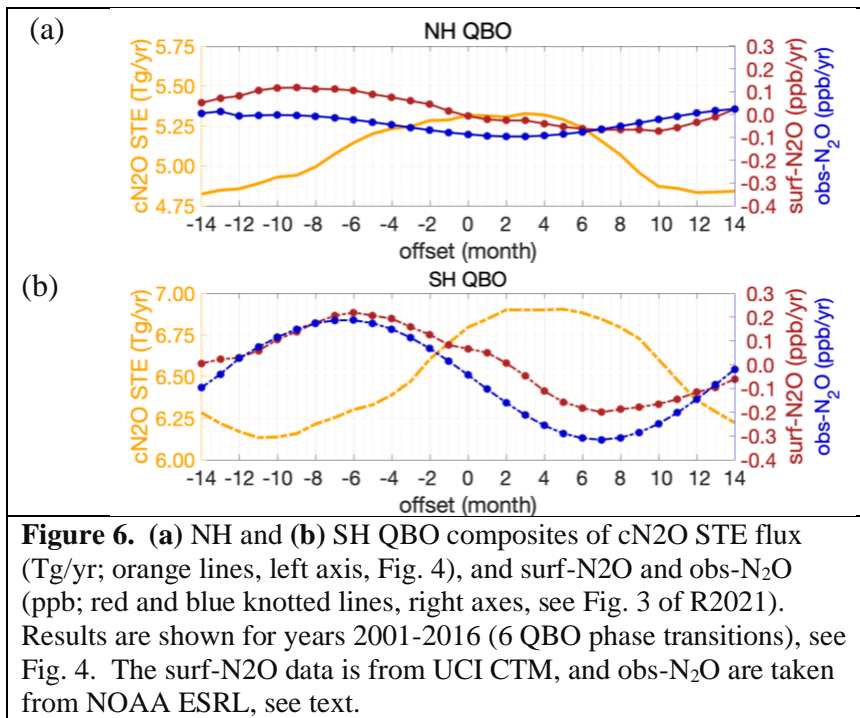
The QBO composite of hemispheric mean cN<sub>2</sub>O STE flux from Figure 4 is compared with the composite of surface abundances (surf-N<sub>2</sub>O and obs-N<sub>2</sub>O) in Figure 6. The peak in cN<sub>2</sub>O flux is broad and flat, but centers on +2 months for the NH and +4 months for the SH. Unlike the annual cycle, the QBO cycle in STE flux is almost in phase in both hemispheres, with the NH preceding the SH. This phasing of the QBO cycle in surface N<sub>2</sub>O was seen with the three models in R2021. In both hemispheres, the modeled surf-N<sub>2</sub>O peaks before the rise in cN<sub>2</sub>O flux and then decreases through most of the period with elevated cN<sub>2</sub>O flux as expected. The amplitude of the QBO STE flux is smaller in the NH than SH by about half, and the amplitude of surf-N<sub>2</sub>O is likewise smaller. The ratio of the amplitudes of surf-N<sub>2</sub>O to cN<sub>2</sub>O STE flux is similar in both hemispheres (~ 0.4 ppb per Tg/yr), which is encouraging. This ratio is larger than the corresponding one from the annual cycles (~ 0.1 ppb per Tg/yr) because the length of the QBO cycle leads to longer accumulation of N<sub>2</sub>O-depleted air from the cN<sub>2</sub>O flux.

In the SH, where the QBO cycle in cN<sub>2</sub>O flux has a large amplitude, the modeled surf-N<sub>2</sub>O matches obs-N<sub>2</sub>O in amplitude and phase as reported in R2021. In the NH, the comparison of

403 surf-N<sub>2</sub>O with obs-N<sub>2</sub>O is not so good: obs-N<sub>2</sub>O has a much smaller amplitude and a different  
 404 phase. This QBO cycle pattern is similar, but reversed, to that of the annual cycle and can be  
 405 understood in the same way. The NH QBO cycle has relatively small amplitude and thus the  
 406 interference with the large-amplitude annual cycle adds noise, obscuring the QBO cycle. In the  
 407 SH it is the opposite, with its weak annual cycle, the SH QBO cycle is clear. The modeled cN<sub>2</sub>O  
 408 fluxes enable us to understand the large-scale variability of the observations.

409  
 410 Thus, for both annual and QBO fluctuations, when the variation in STE flux is dominated by  
 411 either cycle, the surface variations are clearly seen and modeled for that cycle. This further  
 412 supports the findings in R2021 and other studies, that hemispheric surface N<sub>2</sub>O variability is  
 413 driven by stratospheric loss on annual (NH) and QBO (SH) cycles, and it is clearly tied to the  
 414 STE flux. Given the connection between O<sub>3</sub> and cN<sub>2</sub>O STE, this relational metric can be used to  
 415 constrain the O<sub>3</sub> STE for a model ensemble.

416



417

418

419

## 5. Lowermost stratosphere

420 If we accept that matching the observed annual and QBO cycles in surface N<sub>2</sub>O constrains the  
 421 modeled STE cN<sub>2</sub>O flux, then how can we use that to also constrain the modeled STE O<sub>3</sub> flux?  
 422 All evidence, theoretical, observational, and modeled, shows that the STE flux is simultaneous  
 423 for all species (e.g., Figure 1) and in proportion to their relative abundances (i.e., tracer:tracer  
 424 slopes) in the lowermost stratosphere, defined roughly as the region 100-200 hPa in each  
 425 hemisphere outside the tropics (Plumb and Ko, 1992).

426

### 5.1. The O<sub>3</sub>:N<sub>2</sub>O slopes and STE fluxes

427

428

429 We can test the Plumb and Ko hypothesis in our model framework by comparing the relative  
430 STE fluxes for O<sub>3</sub>, cN<sub>2</sub>O and cF11 with the modeled tracer-tracer slopes in the lowermost  
431 stratosphere. These slopes can then be tested using SCISAT-1 ACE-FTS (Scientific Satellite-1  
432 Atmospheric Chemistry Experiment-Fourier Transform Spectrometer) measurements of O<sub>3</sub> and  
433 N<sub>2</sub>O in the lowermost stratosphere to establish the ratio of the two STE fluxes. The ACE-FTS  
434 O<sub>3</sub>:N<sub>2</sub>O slopes were used for model transport and chemistry evaluation (Hegglin and Shepherd,  
435 2007) and found to be very sensitive to satellite sampling, except in the lowermost stratosphere.

436  
437

438 Figure 7ab shows the N<sub>2</sub>O-O<sub>3</sub> slope in each hemisphere taken from the ACE climatology dataset  
439 and the UCI CTM. The current ACE dataset (version 3.5) has been curated from measurements  
440 made by ACE-FTS from February 2004 to February 2013 (Koo et al., 2017). The SCISAT orbit  
441 results in irregular season-latitude coverage, and thus we average the lowermost stratosphere  
442 data over a wide range of latitudes centered on the peak STE flux (20°-60° in both hemispheres).  
443 For both ACE data and the CTM we keep to the lowermost stratosphere (200-100 hPa) and  
444 average over the 4-month peak of STE flux, Feb-May in the NH and Sep-Dec in the SH (see  
445 Figure 1). Extending into the upper tropical troposphere at 20° helps define the tropospheric  
446 end-point of the slope (low O<sub>3</sub>, high N<sub>2</sub>O). Our method described here for deriving the slopes  
447 from the ACE-FTS data is slightly different from that of Hegglin and Shepherd (2007; e.g., we  
448 do not anchor the tropospheric point), and we have the advantage of a longer record.

449  
450

451 Based on the long-term mean STE fluxes in the model, we would expect an O<sub>3</sub>:N<sub>2</sub>O slope of  
452 about -24 (ppb/ppb) in the NH and -17 in the SH. The slopes fitted to our modeled grid-cell  
453 values of O<sub>3</sub> and N<sub>2</sub>O in the lowermost stratosphere are remarkably similar: -23.2 (NH) and -  
454 17.5 (SH). The ACE data are more scattered but show similar, smaller slopes of -19.4 (NH) and  
455 -15.3 (SH). Thus, the NH-SH asymmetry in O<sub>3</sub> versus N<sub>2</sub>O STE fluxes is clearly reflected in the  
456 tracer-tracer slopes, both modeled and observed. Hegglin and Shepherd (2007) had already  
457 identified these NH:SH differences when comparing their model to the ACE-FTS observations  
458 (their Fig. 13cd), but implications for STE fluxes were not brought forward.

459

460 In the modeled SH (Figure 7b), one can see strings of points that are samples along neighboring  
461 cells and reflect a linear mixing line between two different end points, one of which has  
462 experienced extensive O<sub>3</sub> depletion (i.e., the Antarctic O<sub>3</sub> hole). We know that there is some  
463 chemical loss of O<sub>3</sub> in the NH lowermost polar stratosphere during very cold winters (Manney et  
464 al., 2011; Isaksen et al., 2012), but it is not extensive enough to systematically affect the O<sub>3</sub>:N<sub>2</sub>O  
465 slope over the mid-latitude lowermost stratosphere in either the ACE observations or the CTM  
466 simulations.

467

468

469

470

471

472

473

474

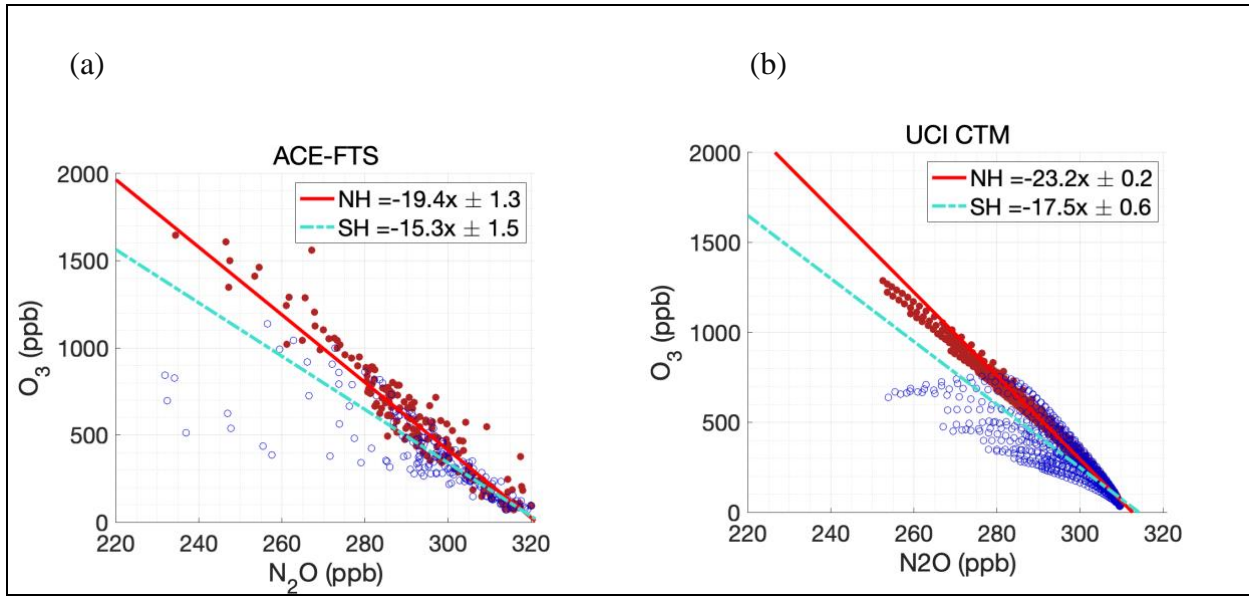


**Figure 7.** O<sub>3</sub> versus N<sub>2</sub>O (x-axis) scatter plots from (a) SCISAT ACE-FTS and (b) the UCI CTM. ACE-FTS data is from monthly climatologies for the period Feb 2004 to Feb 2013 restricted to 200-100 hPa, latitudes about 20°-60°, and months Feb-May (NH, red) or Sep-Dec (SH, blue). The linear-fit lines (ppb/ppb, values in legend) are restricted to larger N<sub>2</sub>O values (>280 ppb) to more accurately represent the STE fluxes, see Olsen et al. (2001).

475  
 476  
 477  
 478  
 479  
 480  
 481  
 482  
 483  
 484  
 485  
 486  
 487  
 488  
 489  
 490  
 491  
 492  
 493  
 494  
 495  
 496  
 497  
 498  
 499  
 500

### 5.2. IAV of the Antarctic ozone hole and the SH STE O<sub>3</sub> flux

The Antarctic ozone hole appears to be the source of the NH-SH asymmetry in the STE fluxes of O<sub>3</sub> versus N<sub>2</sub>O. It is known that the massive chemical depletion of O<sub>3</sub> inside the Antarctic vortex between about 13 and 23 km altitude creates an air mass with lower O<sub>3</sub>:N<sub>2</sub>O ratios than usually found in the mid-latitude lowermost stratosphere. When the vortex breaks up, nominally in late November, much of this O<sub>3</sub>-depleted air can mix along isentropes into the mid-latitude lowermost stratosphere, changing the O<sub>3</sub>:N<sub>2</sub>O ratios and reducing the SH STE O<sub>3</sub> flux.

We have additional information on the SH O<sub>3</sub> STE flux from the year-to-year variations in the size of the ozone hole. The best measure of the scale of Antarctic ozone depletion is the October mean ozone column (DU) averaged from the pole to 63°S equivalent latitude (see Fig. 4-5 of WMO, 2018). When we compare the CTM with the observations (Figure 8), we find remarkable verisimilitude in the model: the root-mean-squared difference is 9 DU out of a standard deviation of 29 DU and the correlation coefficient is 0.96. Thus, we have confidence that we are simulating the correct IAV of the ozone hole. Next, we plot the modeled O<sub>3</sub> STE flux (summed over the 12 months following the peak ozone hole, November-October) with the modeled October ozone column and find a fairly linear relationship. If we estimate the STE O<sub>3</sub> flux



501 before the O<sub>3</sub> hole, when the mean October O<sub>3</sub> column was about 307 DU, then our O<sub>3</sub> flux  
502 increases to 209 Tg/yr (see Figure 8, red marker), eliminating the hemispheric asymmetry in O<sub>3</sub>  
503 STE flux.

504  
505 The annual deficit in SH STE O<sub>3</sub> flux brought on by the Antarctic ozone hole ranges from about  
506 5 to 55 Tg/yr and with a central value of 30 Tg/yr or 14% of the total. Using the decadal trends  
507 1965-2000 from Hegglin and Shepherd (2009), this deficit is 8%; and from Meul et al. (2018),  
508 5%. Since both of these models calculate a much larger SH flux (~300 Tg/yr), we estimate their  
509 absolute change in O<sub>3</sub> flux to be 24 and 15 Tg/yr, respectively. Because the ozone hole  
510 effectively removes a fixed, rather than proportional, amount of ozone that presumably is  
511 mapped onto the STE flux the following year, we believe the absolute change is the best  
512 measure. Thus the three models estimate the ozone hole causes a deficit in the SH O<sub>3</sub> STE flux  
513 in the range of 15-30 Tg/yr. The UCI CTM's ability to match the observed IAV of the ozone  
514 hole, and to match that linearly with the deficit in STE flux provides support for the upper end of  
515 the range. Note that the difference in O<sub>3</sub>:N<sub>2</sub>O slopes between NH and SH in Figure 7 is about 5.  
516 If we attribute that solely to the ozone hole and split the flux of N<sub>2</sub>O-depleted air evenly between  
517 hemispheres, then the ozone-hole-driven O<sub>3</sub> STE flux difference is about 55 Tg/yr, about twice  
518 that derived from the variability in our model. This difference in estimated flux indicates that  
519 even without chlorine-driven ozone depletion, the O<sub>3</sub>:N<sub>2</sub>O slopes may be inherently different  
520 simply because of the strong descent inside the wintertime Antarctic vortex. This can be readily  
521 investigated with further model studies.

522  
523 We looked for any relationship between ozone hole IAV and the STE fluxes of cN<sub>2</sub>O or cF11  
524 and found mostly a scatter plot with no clear relationship. Given the analysis above, we expect  
525 that much of the scatter is related to QBO cycles.

526  
527

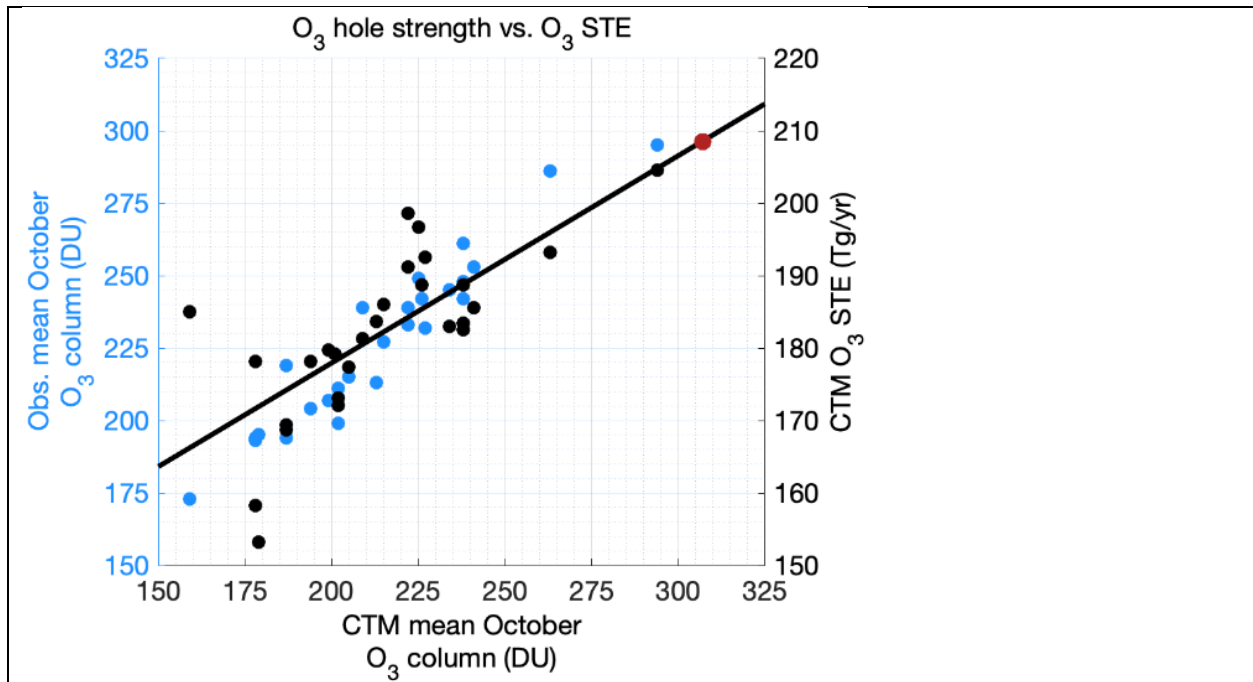


**Figure 8.** Interannual variability of the observed Antarctic ozone hole from 1990 to 2017 (blue dots; left y-axis) versus the CTM modeled ozone hole (x-axis); plus the CTM modeled SH STE O<sub>3</sub> flux (black dots; right y-axis) versus the modeled ozone hole (x-axis). The ozone hole is measured by the total ozone column (DU) averaged daily over October poleward of 63°S in equivalent latitude (see Figure 4.5 of WMO 2018). The SH STE O<sub>3</sub> flux (Tg/yr) is centered on May 1 of the following year (i.e., the 12 months following the nominal breakup of the ozone hole). The black line is a simple regression fit of the modeled STE to the modeled ozone hole (black dots), and the red dot is our estimate of pre-ozone-hole SH STE O<sub>3</sub> flux based on the observed 1979-82 O<sub>3</sub> column.

528  
529  
530  
531  
532  
533  
534  
535  
536  
537  
538  
539  
540

### 5.3 Other model-measurement metrics related to STE

What else might affect O<sub>3</sub> STE? Stratospheric column O<sub>3</sub> (DU) varies on annual and QBO timescales. These changes in O<sub>3</sub> overhead can have a direct influence on O<sub>3</sub> transport to the troposphere, but the link requires further analysis. Tang et al. (2021) showed the UCI CTM is able to capture the observed annual cycle of stratospheric O<sub>3</sub> column as extracted from total column using the Ziemke et al. (2019) method. QBO modulation of stratospheric column O<sub>3</sub> has not been fully investigated since Tung and Yang (1994b). Yet, the fluctuations in mass over the annual cycle are comparable to the corresponding variability in O<sub>3</sub> STE flux (1 DU = 10.9 Tg) and likely connected (Figure 9).

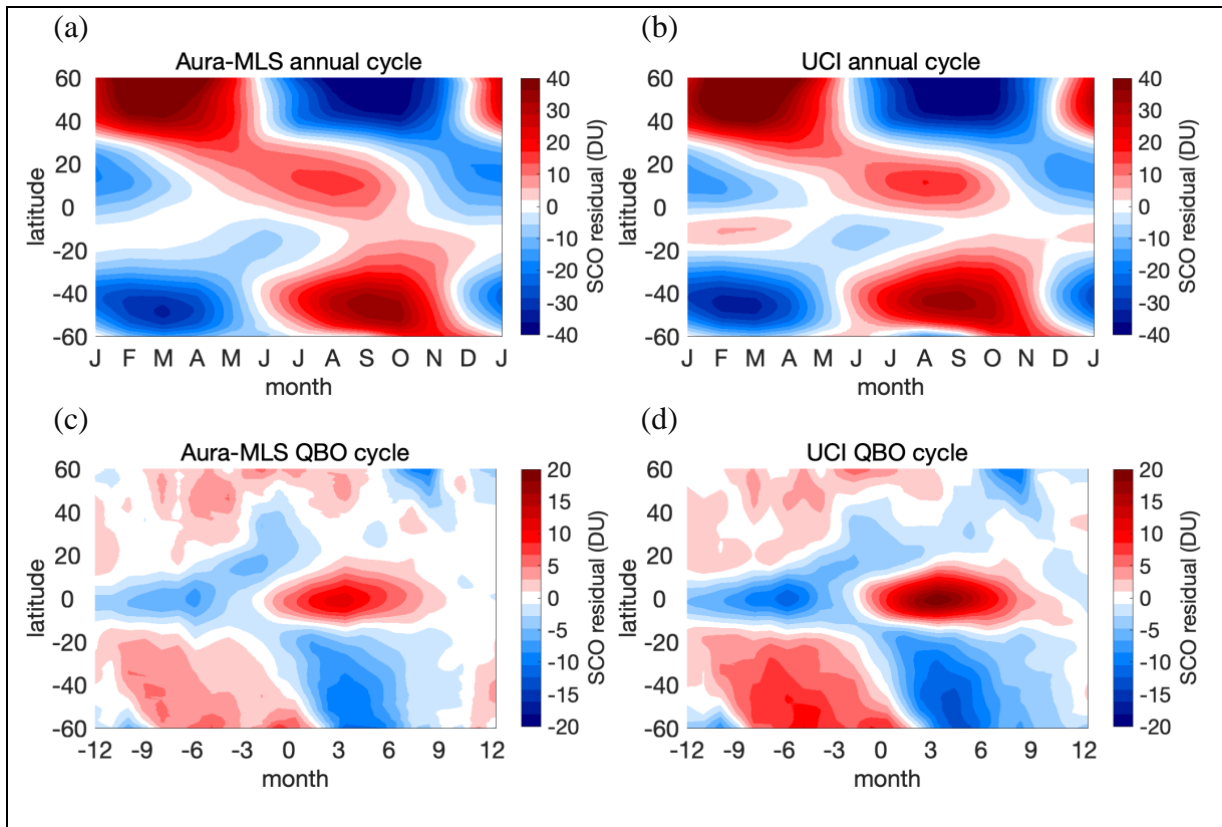


**Figure 9.** Stratospheric O<sub>3</sub> column residuals taken from Aura-MLS (a, c) and UCI CTM (b, d) for their mean annual cycle (a, b) and mean QBO cycle (c, d) during years 2005-2017. Residuals are defined at each latitude with a mean of zero DU.

541

542  
543  
544  
545  
546  
547  
548  
549  
550  
551  
552  
553  
554  
555

## 6. Conclusions

This work examines how closely O<sub>3</sub> STE is linked to STE fluxes of other trace gases. By including our complementary N<sub>2</sub>O and F11 tracers, we can follow stratospheric loss of these gases along with stratospheric O<sub>3</sub> across the tropopause. The magnitudes of the fluxes are proportional to their abundances in the lower stratosphere as expected (Plumb and Ko, 1992), and their variability is highly correlated with one another, indicating that they are entering the troposphere simultaneously. Even the distinct QBO pattern of STE fluxes is consistent across O<sub>3</sub>, N<sub>2</sub>O and F11. We further constrain the N<sub>2</sub>O transport pathway by linking STE of depleted-N<sub>2</sub>O air with surface fluctuations of N<sub>2</sub>O abundance. The surface response in modeled N<sub>2</sub>O matches well with the observed surface variability in the SH, indicating that surface variability is driven largely by STE flux.

*Consistency of STE O<sub>3</sub> flux.* As summarized here, there are a number of model diagnostics and observational constraints that provide a reality check on the consistency of the modeled O<sub>3</sub> STE flux. In Table 1, we examine these for our model and also for the CMAM model (Hegglin and Shepherd, 2007, 2009) because it is one of the few with enough published results. For UCI we calculate NH:SH fluxes of O<sub>3</sub> (208:182 Tg-O<sub>3</sub>/yr) and N<sub>2</sub>O (5.1:6.4 Tg-N/yr). Thus the mole fraction slopes in the lowermost stratosphere should be -23.8 (NH) and -16.6 (SH). Our model O<sub>3</sub>:N<sub>2</sub>O slopes are -23.2 (NH) and -17.5 (SH). Given the seasonal variability and scatter in the correlation plots (Figure 7), we count this as consistent. For CMAM, the modeled O<sub>3</sub>:N<sub>2</sub>O slopes, -23±2 (NH) and -18±3 (SH) are similar to ours and also to the ACE-FTS observations as analyzed by Hegglin and Shepherd (2007), -22±4 (NH) and -14±3 (SH), or by us, -19 (NH) and -15 (SH). CMAM does not report the implied STE N<sub>2</sub>O fluxes derived from their photochemical loss of N<sub>2</sub>O, but their model seems to match observations of N<sub>2</sub>O in the middle stratosphere, and so we assume that the Aura-MLS derived N<sub>2</sub>O fluxes are a close estimate (12.9 Tg-N/yr). Note we are using Aura-MLS N<sub>2</sub>O values here to calculate the photochemical loss, which occurs in the middle to upper stratosphere (see R2021 for methodology). Just using the CMAM global numbers for O<sub>3</sub> STE flux, we calculate the O<sub>3</sub>:N<sub>2</sub>O slope in the lowermost stratosphere should average to -30. We conclude that their diagnosis of the STE O<sub>3</sub> flux, 655 Tg/yr, is inconsistent with the circulation that generated the O<sub>3</sub>:N<sub>2</sub>O slopes and is 50% too large. We do not view this as a critical assessment of CMAM since it involves us combining diagnostics from two separate publications and possibly different model simulations, but it is an example of how we might expect future studies of the STE O<sub>3</sub> flux to self-evaluate.

*Uncertainty Quantification in STE O<sub>3</sub> flux.* Deriving a best estimate and uncertainty from this work involves expert judgment. Changes in meteorological data used by the UCI CTM (IFS Cycles 29r1, 36r1, and 38r1, all at 60-layer 1.1° resolution, see Table 1) give a standard deviation in STE of 13% (only 3 values). If we use observations to derive a value as in Murphy and Fahey (1994), we must expand our dimensions to the uncertainty in the NH:SH split of N<sub>2</sub>O flux to calculate each hemisphere's O<sub>3</sub> flux. The factors are: (1) total STE N<sub>2</sub>O flux is 12.9 Tg-N/yr from the Aura-MLS data and we assign a ±10% one-sigma uncertainty; (2) the NH:SH split of the N<sub>2</sub>O flux is 44:56 in our current model, was not diagnosed for previous ones, and so we assume a value of 50:50 that ranges from 40:60 to 60:40; (3) analysis of the ACE-FTS observations (ours and Hegglin and Shepherd, 2007) gives O<sub>3</sub>:N<sub>2</sub>O slopes of about -21 (NH) and

588 -15 (SH) to which we assign a one-sigma uncertainty of  $\pm 3$ . Propagating these as root-mean  
 589 square errors, we find a  $\pm 15\%$  uncertainty in the global value,  $400 \pm 60$  Tg/yr. Uncertainty in the  
 590 hemispheric values is more difficult to assess, and from a range of model results shown in Table  
 591 1, we can only estimate that the NH:SH ratio is between 60:40 and 50:50, a range that bounds  
 592 our and CMAM results plus 2%. Note that this estimate is for current conditions with a regularly  
 593 occurring Antarctic ozone hole. We believe the low 50:50 ratio is plausible because we have  
 594 shown that our large SH STE N<sub>2</sub>O flux is consistent with the surface QBO variability in N<sub>2</sub>O.  
 595 For pre-1980, and for when the ozone hole recovers later this century, we anticipate that the SH  
 596 O<sub>3</sub>:N<sub>2</sub>O slope will revert to -18 to -21, and the total STE O<sub>3</sub> flux to 430-460 Tg/yr. This  
 597 simplistic estimate is based on a fixed atmospheric circulation.  
 598

599 A major surprise from our model is that the STE flux of O<sub>3</sub> is predominantly NH biased  
 600 currently, only because of the Antarctic ozone hole. Prior to 1980, and after 2060, it would/will  
 601 be symmetric between the hemispheres. Our model calculates slightly greater STE fluxes for  
 602 trace gases like N<sub>2</sub>O or F11 in the SH, which is counter to prevailing theory that the wave-driven  
 603 fluxes force relatively greater STE in the NH. This difference cannot be directly tested with  
 604 observations of trace gases, but a range of N<sub>2</sub>O hemispheric observations are well modeled and  
 605 support this premise. More extensive work with multi-model ensembles that include both  
 606 chemical and dynamical diagnostics in the stratosphere would be needed to overturn the  
 607 established theory. Our work reemphasizes the importance of trace-gas correlations in the  
 608 lowermost stratosphere as a key observational metric for climate models that may be able to  
 609 constrain total STE fluxes. The tracer slopes may go beyond just relative STE fluxes because we  
 610 have other measurements from the upper stratosphere to the surface that constrain, for example,  
 611 the absolute flux of N<sub>2</sub>O better than we first did using just the modeled lifetime.  
 612

613 In Table 2, we gather a set of observation-based model metrics that relate to STE fluxes and will  
 614 help the community build more robust models to better derive the STE flux of O<sub>3</sub>.  
 615

<b>Table 1.</b> Summary of key results for the STE flux of O <sub>3</sub> and N <sub>2</sub> O presented here (bold)				
	NH	SH	Global	notes
STE O <sub>3</sub> flux (TgO <sub>3</sub> /yr)	<b>208</b>	<b>182</b>	<b>390</b>	IFS Cy38r1, yrs 1990-2017 (this paper; Ruiz et al., 2021)
	239	198	437	IFS Cy36r1, yrs 2000-2007 (Hsu & Prather, 2014)
	301	233	534	IFS Cy29r1, yrs 2000-2006 (Hsu & Prather, 2014)
	383	272	655	CMAM, yrs 1995-2005 (Hegglin & Shepherd, 2009)
STE N <sub>2</sub> O flux (TgN/yr)	<b>5.1</b>	<b>6.4</b>	<b>11.5</b>	yrs 1990-2017, scaled to 320 ppb
			<b>12.9</b>	using Aura-MLS lifetime of 119 yr and 320 ppb
LMS O <sub>3</sub> :N <sub>2</sub> O slope*	<b>-23.2</b>	<b>-17.5</b>		UCI model
	<b>-19.4</b>	<b>-15.3</b>		ACE-FTS observations
	-23 $\pm$ 2	-18 $\pm$ 3		CMAM model, Fig 13 of (Hegglin & Shepherd, 2007)
	-22 $\pm$ 4	-14 $\pm$ 3		ACE-FTS observations, ibid
			-20.0	(Murphy & Fahey, 1994)
			-22.0	(McLinden et al., 2000)

STE flux O <sub>3</sub> :N <sub>2</sub> O (mole/mole)	<b>-23.8</b>	<b>-16.6</b>		UCI model, calculated from entries above
			-29.6	CMAM (Hegglin & Shepherd, 2009), using Aura-MLS N <sub>2</sub> O lifetime
Best Estimate STE O <sub>3</sub> flux (Tg/yr)	<b>60% to 50%</b>	<b>40% to 50%</b>	<b>400 ± 60</b>	current Antarctic ozone hole conditions, see text
* LMS = lowermost stratosphere only. For UCI model, months are selected for highest STE (FMAM in NH, SON in SH, Fig. 1). For CMAM, the monthly ranges from their Fig. 13cd are estimated. Where no reference is given, the source is this paper.				

616  
617

<b>Table 2.</b> Metrics from Measurements or Constrained Values for CCMs related to Stratosphere-Troposphere Exchange				
<i>Name</i>	<i>Metric</i>	<i>Measured values</i>	<i>Model requirements</i>	<i>Example figure</i>
N <sub>2</sub> O loss	Annual and QBO cycles of global mean stratospheric N <sub>2</sub> O loss	Monthly N <sub>2</sub> O loss calculated from Aura-MLS profiles (2005-present)	Stratospheric chemistry for N <sub>2</sub> O as tracer; a QBO cycle; monthly mean diagnostics	Fig. 4 (Prather et al., 2015); Fig. 2 (Ruiz et al., 2021); Fig. 3 (this paper)
STE slopes	Matching O <sub>3</sub> :N <sub>2</sub> O slopes in lowermost stratosphere	ACE FTS profiles (2004-2013)	Stratospheric O <sub>3</sub> and N <sub>2</sub> O calculation, possibly also CFCs; monthly snapshots	Fig. 7 (this paper)
Strat O <sub>3</sub> column	Annual and QBO composite cycles of stratospheric O <sub>3</sub> column	Monthly zonal mean stratospheric O <sub>3</sub> column from Ziemke et al., 2019 (2005-present)	Stratospheric O <sub>3</sub> chemistry; a QBO cycle; monthly mean diagnostics; separate strat & trop O <sub>3</sub> columns	Fig. 9 (this paper)
N <sub>2</sub> O loss at surface	Annual and QBO composite cycles of surface N <sub>2</sub> O solely from stratospheric loss	NOAA surface N <sub>2</sub> O observations	Stratospheric N <sub>2</sub> O chemistry; N <sub>2</sub> O as a tracer; monthly mean diagnostics	Fig. 3 (Ruiz et al., 2021); Fig. 5 (this paper)
		<i>Constrained (modeled) values</i>		
STE flux of O <sub>3</sub>		Monthly, latitude or hemispheric resolved, net O <sub>3</sub> flux	Run O3strat as a tracer; diagnose monthly flux into troposphere, at tropopause or through trop- loss of O3strat	Fig. 1 & 2 (this paper)
STE flux of N <sub>2</sub> O depleted air (also CFC-11)		Monthly, latitude or hemispheric resolved, STE flux of N <sub>2</sub> O (CFC-11)	Run cN2O (cF11) as a tracer; diagnose monthly flux into troposphere	Fig. 1 & 2 (this paper);
SH O <sub>3</sub> hole and flux		Change in SH O <sub>3</sub> STE flux with size of ozone hole; observed IAV of O <sub>3</sub> hole	IAV of ozone hole; daily total O <sub>3</sub> column (lat, long); monthly SH O <sub>3</sub> STE flux	Fig 7 (this paper)
Notes: Constrained values are model-only derived quantities that can be diagnosed from CCMs or CTMs.				

618  
619  
620  
621  
622

623  
624  
625  
626  
627  
628  
629  
630  
631  
632  
633  
634  
635  
636  
637  
638  
639  
640  
641  
642  
643  
644  
645  
646  
647  
648  
649  
650  
651  
652  
653  
654  
655  
656  
657  
658  
659  
660  
661  
662  
663  
664  
665  
666

**Author Contributions:**

DJR and MJP designed and carried out the study and prepared the manuscript for publication.

**Competing interests:**

The authors declare that they have no conflict of interest.

**Acknowledgments:**

Research at UCI was supported by grants from the National Aeronautics and Space Administration’s Modeling, Analysis and Prediction Program (award NNX13AL12G), and Atmospheric Chemistry Modeling and Analysis Program (80NSSC20K1237, NNX15AE35G), and the National Science Foundation (NRT-1633631). We gratefully acknowledge the work of the MLS team in producing the Level 3 data sets that enabled our MLS-related analyses. Work at the Jet Propulsion Laboratory, California Institute of Technology, was performed under contract with the National Aeronautics and Space Administration. We thank the ACE-FTS team for making the climatology data used here available for our analyses. The Atmospheric Chemistry Experiment (ACE), also known as SCISAT, is a Canadian-led mission mainly supported by the Canadian Space Agency. We also acknowledge Ed Dlugokencky for providing the surface N<sub>2</sub>O data that was used here to produce an observation-based reference with which to compare our simulated results. The data used to produce the figures and tables in this work are accessible via the DRYAD repository with DOI <https://doi.org/10.7280/D1JX0K>

667  
668  
669  
670  
671  
672  
673  
674  
675  
676  
677  
678  
679  
680  
681  
682  
683  
684  
685  
686  
687  
688  
689  
690  
691  
692  
693  
694  
695  
696  
697  
698  
699  
700  
701  
702  
703  
704  
705  
706  
707  
708

**References:**

Appenzeller, C., Holton, J. R., and Rosenlof, K. H.: Seasonal variation of mass transport across the tropopause, *J Geophys Res-Atmos*, 101, 15071-15078, doi:10.1029/96JD00821, 1996.

Baldwin, M. P., Gray, L. J., Dunkerton, T. J., Hamilton, K., Haynes, P. H., Randel, W. J., Holton, J. R., Alexander, M. J., Hirota, I., Horinouchi, T., Jones, D. B. A., Kinnersley, J. S., Marquardt, C., Sato, K., and Takahashi, M.: The quasi-biennial oscillation, *Reviews of Geophysics*, 39, 179-229, 2001.

Butterbach-Bahl, K., Baggs, E. M., Dannenmann, M., Kiese, R., and Zechmeister-Boltenstern, S.: Nitrous oxide emissions from soils: how well do we understand the processes and their controls?, *Philos T R Soc B*, 368, 10.1098/rstb.2013.0122, 2013.

Dlugokencky, E. J., Crotwell, A. M., Mund, J. W., Crotwell, M. J., and Thoning, K. W.: Atmospheric Nitrous Oxide Dry Air Mole Fractions from the NOAA ESRL Carbon Cycle Cooperative Global Air Sampling Network, 1997-2018, Version: 2019-07, 10.15138/53g1-x417, 2019.

Gottelman, A., Holton, J. R., and Rosenlof, K. H.: Mass fluxes of O-3, CH4, N2O and CF2Cl2 in the lower stratosphere calculated from observational data, *J Geophys Res-Atmos*, 102, 19149-19159, Doi 10.1029/97jd01014, 1997.

Griffiths, P. T., Murray, L. T., Zeng, G., Shin, Y. M., Abraham, N. L., Archibald, A. T., Deushi, M., Emmons, L. K., Galbally, I. E., Hassler, B., Horowitz, L. W., Keeble, J., Liu, J., Moeini, O., Naik, V., O'Connor, F. M., Oshima, N., Tarasick, D., Tilmes, S., Turnock, S. T., Wild, O., Young, P. J., and Zanis, P.: Tropospheric ozone in CMIP6 simulations, *Atmos Chem Phys*, 21, 4187-4218, 10.5194/acp-21-4187-2021, 2021.

Hamilton, K., and Fan, S. M.: Effects of the stratospheric quasi-biennial oscillation on long-lived greenhouse gases in the troposphere, *J Geophys Res-Atmos*, 105, 20581-20587, 10.1029/2000jd900331, 2000.

Hegglin, M. I., and Shepherd, T. G.: Large climate-induced changes in ultraviolet index and stratosphere-to-troposphere ozone flux, *Nature Geoscience*, 2, 687-691, Doi 10.1038/Ngeo604, 2009.

Hegglin, M. I., and Shepherd, T. G.: O3-N2O correlations from the Atmospheric Chemistry Experiment: Revisiting a diagnostic of transport and chemistry in the stratosphere, *J Geophys Res-Atmos*, 112, Artn D19301, 10.1029/2006jd008281, 2007.

Hess, P., Kinnison, D., and Tang, Q.: Ensemble simulations of the role of the stratosphere in the attribution of northern extratropical tropospheric ozone variability, *Atmos Chem Phys*, 15, 2341-2365, 10.5194/acp-15-2341-2015, 2015.

709 Hirsch, A. I., Michalak, A. M., Bruhwiler, L. M., Peters, W., Dlugokencky, E. J., and Tans, P. P.:  
710 Inverse modeling estimates of the global nitrous oxide surface flux from 1998-2001, *Global*  
711 *Biogeochem Cy*, 20, Artn Gb1008, 10.1029/2004gb002443, 2006.

712 Holton, J. R., Haynes, P. H., McIntyre, M. E., Douglass, A. R., Rood, R. B., and Pfister, L.:  
713 Stratosphere-Troposphere Exchange, *Reviews of Geophysics*, 33, 403-439, 1995.

714 Holton, J. R.: On the Global Exchange of Mass between the Stratosphere and Troposphere, *J*  
715 *Atmos Sci*, 47, 392-395, Doi 10.1175/1520-0469(1990)047<0392:Otgeom>2.0.Co;2, 1990.

716 Hsu, J. N., and Prather, M. J.: Is the residual vertical velocity a good proxy for stratosphere-  
717 troposphere exchange of ozone?, *Geophys Res Lett*, 41, 9024-9032,  
718 10.1002/2014GL061994, 2014.

719 Hsu, J., and Prather, M. J.: Global long-lived chemical modes excited in a 3-D chemistry  
720 transport model: Stratospheric N<sub>2</sub>O, NO<sub>y</sub>, O<sub>3</sub> and CH<sub>4</sub> chemistry, *Geophys Res Lett*, 37,  
721 L07805, Artn L07805, 10.1029/2009gl042243, 2010.

722 Hsu, J., and Prather, M. J.: Stratospheric variability and tropospheric ozone, *J Geophys Res-*  
723 *Atmos*, 114, Artn D06102, 10.1029/2008jd010942, 2009.

724 Hsu, J., Prather, M. J., and Wild, O.: Diagnosing the stratosphere-to-troposphere flux of ozone in  
725 a chemistry transport model, *J Geophys Res-Atmos*, 110, Artn D19305,  
726 10.1029/2005jd006045, 2005.

727 Isaksen, I. S. A., Zerefos, C., Wang, W. C., Balis, D., Eleftheratos, K., Rognerud, B., Stordal, F.,  
728 Berntsen, T. K., LaCasce, J. H., Sovde, O. A., Olivie, D., Orsolini, Y. J., Zyrichidou, I.,  
729 Prather, M., and Tuinder, O. N. E.: Attribution of the Arctic ozone column deficit in March  
730 2011, *Geophys Res Lett*, 39, Artn L24810, 10.1029/2012gl053876, 2012.

731 Kinnersley, J. S., and Tung, K. K.: Mechanisms for the extratropical QBO in circulation and  
732 ozone, *J Atmos Sci*, 56, 1942-1962, Doi 10.1175/1520-  
733 0469(1999)056<1942:Mfteqi>2.0.Co;2, 1999.

734 Koo, J. H., Walker, K. A., Jones, A., Sheese, P. E., Boone, C. D., Bernath, P. F., & Manney, G.  
735 L.: Global climatology based on the ACE-FTS version 3.5 dataset: Addition of mesospheric  
736 levels and carbon-containing species in the UTLS. *Journal of Quantitative Spectroscopy and*  
737 *Radiative Transfer*, 186, 52–62, 10.1016/j.jqsrt.2016.07.003, 2017.

738 Liang, Y. X., Gillett, N. P., and Monahan, A. H.: Climate Model Projections of 21st Century  
739 Global Warming Constrained Using the Observed Warming Trend, *Geophys Res Lett*, 47,  
740 ARTN e2019GL086757, 10.1029/2019GL086757, 2020.

741 Liu, H. Y., Considine, D. B., Horowitz, L. W., Crawford, J. H., Rodriguez, J. M., Strahan, S. E.,  
742 Damon, M. R., Steenrod, S. D., Xu, X. J., Kouatchou, J., Carouge, C., and Yantosca, R. M.:  
743 Using beryllium-7 to assess cross-tropopause transport in global models, *Atmos Chem Phys*,  
744 16, 4641-4659, 10.5194/acp-16-4641-2016, 2016.

745 Manney, G. L., Santee, M. L., Rex, M., Livesey, N. J., Pitts, M. C., Veefkind, P., Nash, E. R.,  
746 Wohltmann, I., Lehmann, R., Froidevaux, L., Poole, L. R., Schoeberl, M. R., Haffner, D. P.,  
747 Davies, J., Dorokhov, V., Gernandt, H., Johnson, B., Kivi, R., Kyro, E., Larsen, N., Levelt,  
748 P. F., Makshtas, A., McElroy, C. T., Nakajima, H., Parrondo, M. C., Tarasick, D. W., von  
749 der Gathen, P., Walker, K. A., and Zinoviev, N. S.: Unprecedented Arctic ozone loss in  
750 2011, *Nature*, 478, 469-U465, 10.1038/nature10556, 2011.

751 McLinden, C. A., Olsen, S. C., Hannegan, B., Wild, O., Prather, M. J., and Sundet, J.:  
752 Stratospheric ozone in 3-D models: A simple chemistry and the cross-tropopause flux, *J*  
753 *Geophys Res-Atmos*, 105, 14653-14665, 10.1029/2000JD900124, 2000.



754 Meul, S., Langematz, U., Kroger, P., Oberlander-Hayn, S., and Jockel, P.: Future changes in the  
755 stratosphere-to-troposphere ozone mass flux and the contribution from climate change and  
756 ozone recovery, *Atmos Chem Phys*, 18, 7721-7738, 10.5194/acp-18-7721-2018, 2018.

757 Montzka, S. A., Dutton, G. S., Yu, P. F., Ray, E., Portmann, R. W., Daniel, J. S., Kuijpers, L.,  
758 Hall, B. D., Mondeel, D., Siso, C., Nance, D., Rigby, M., Manning, A. J., Hu, L., Moore, F.,  
759 Miller, B. R., and Elkins, J. W.: An unexpected and persistent increase in global emissions  
760 of ozone-depleting CFC-11, *Nature*, 557, 413-416, 10.1038/s41586-018-0106-2, 2018.

761 Murphy, D. M., and Fahey, D. W.: An estimate of the flux of stratospheric reactive nitrogen and  
762 ozone into the troposphere, *Journal of Geophysical Research*, 99, 5325-5332, 1994.

763 Nevison, C. D., Kinnison, D. E., and Weiss, R. F.: Stratospheric influences on the tropospheric  
764 seasonal cycles of nitrous oxide and chlorofluorocarbons, *Geophys Res Lett*, 31, Artn  
765 L20103, 10.1029/2004gl020398, 2004.

766 Nevison, C. D., Mahowald, N. M., Weiss, R. F., and Prinn, R. G.: Interannual and seasonal  
767 variability in atmospheric N<sub>2</sub>O, *Global Biogeochem Cy*, 21, Artn Gb3017,  
768 10.1029/2006gb002755, 2007.

769 Newman, P.: The quasi-biennial oscillation (QBO), NASA, Goddard Space Flight Center,  
770 [https://acd-ext.gsfc.nasa.gov/Data\\_services/met/qbo/qbo.html](https://acd-ext.gsfc.nasa.gov/Data_services/met/qbo/qbo.html), retrieved on 3 Mar 2020.

771 Olsen, M. A., Manney, G. L., and Liu, J. H.: The ENSO and QBO Impact on Ozone Variability  
772 and Stratosphere-Troposphere Exchange Relative to the Subtropical Jets, *J Geophys Res-*  
773 *Atmos*, 124, 7379-7392, 10.1029/2019JD030435, 2019.

774 Olsen, M. A., Schoeberl, M. R., and Douglass, A. R.: Stratosphere-troposphere exchange of mass  
775 and ozone, *J Geophys Res-Atmos*, 109, Artn D24114, 10.1029/2004jd005186, 2004.

776 Olsen, S. C., McLinden, C. A., and Prather, M. J.: Stratospheric N<sub>2</sub>O-NO<sub>y</sub> system: testing  
777 uncertainties in a three-dimensional framework, *J. Geophys. Res.*, 106, 28771-28784, 2001.

778 Plumb, R. A., and Ko, M. K. W.: Interrelationships between Mixing Ratios of Long Lived  
779 Stratospheric Constituents, *J Geophys Res-Atmos*, 97, 10145-10156, 1992.

780 Prather, M. J., Hsu, J., DeLuca, N. M., Jackman, C. H., Oman, L. D., Douglass, A. R., Fleming,  
781 E. L., Strahan, S. E., Steenrod, S. D., Sovde, O. A., Isaksen, I. S. A., Froidevaux, L., and  
782 Funke, B.: Measuring and modeling the lifetime of nitrous oxide including its variability, *J*  
783 *Geophys Res-Atmos*, 120, 5693-5705, 10.1002/2015JD023267, 2015.

784 Prather, M. J., Zhu, X., Tang, Q., Hsu, J., and Neu, J. L.: An atmospheric chemist in search of  
785 the tropopause, *J. Geophys. Res.*, 116, D04306, 10.1029/2010jd014939, 2011.

786 Ray, E. A., Portmann, R. W., Yu, P. F., Daniel, J., Montzka, S. A., Dutton, G. S., Hall, B. D.,  
787 Moore, F. L., and Rosenlof, K. H.: The influence of the stratospheric Quasi-Biennial  
788 Oscillation on trace gas levels at the Earth's surface, *Nat Geosci*, 13, 22-24, 10.1038/s41561-  
789 019-0507-3, 2020.

790 Ruiz, D. J., Prather, M. J., Strahan, S. E., Thompson, R. L., Froidevaux, L., and Steenrod, S. D.:  
791 How Atmospheric Chemistry and Transport Drive Surface Variability of N<sub>2</sub>O and CFC-11,  
792 *J Geophys Res-Atmos*, 126, ARTN e2020JD033979, 10.1029/2020JD033979, 2021.

793 Stohl, A., Bonasoni, P., Cristofanelli, P., Collins, W., Feichter, J., Frank, A., Forster, C.,  
794 Gerasopoulos, E., Gaggeler, H., James, P., Kentarchos, T., Kromp-Kolb, H., Kruger, B.,  
795 Land, C., Meloan, J., Papayannis, A., Priller, A., Seibert, P., Sprenger, M., Roelofs, G. J.,  
796 Scheel, H. E., Schnabel, C., Siegmund, P., Tobler, L., Trickl, T., Wernli, H., Wirth, V.,  
797 Zanis, P., and Zerefos, C.: Stratosphere-troposphere exchange: A review, and what we have  
798 learned from STACCATO, *J Geophys Res-Atmos*, 108, Artn 8516, 10.1029/2002jd002490,  
799 2003.

800 Strahan, S. E., Douglass, A. R., Stolarski, R. S., Akiyoshi, H., Bekki, S., Braesicke, P., Butchart,  
801 N., Chipperfield, M. P., Cugnet, D., Dhomse, S., Frith, S. M., Gettelman, A., Hardiman, S.  
802 C., Kinnison, D. E., Lamarque, J. F., Mancini, E., Marchand, M., Michou, M., Morgenstern,  
803 O., Nakamura, T., Olivie, D., Pawson, S., Pitari, G., Plummer, D. A., Pyle, J. A., Scinocca,  
804 J. F., Shepherd, T. G., Shibata, K., Smale, D., Teysse, H., Tian, W., and Yamashita, Y.:  
805 Using transport diagnostics to understand chemistry climate model ozone simulations, *J*  
806 *Geophys Res-Atmos*, 116, ArtD17302, 10.1029/2010jd015360, 2011.

807 Tang, Q., and Prather, M. J.: Correlating tropospheric column ozone with tropopause folds: the  
808 Aura-OMI satellite data, *Atmos Chem Phys*, 10, 9681-9688, 10.5194/acp-10-9681-2010,  
809 2010.

810 Tang, Q., Hess, P. G., Brown-Steiner, B., and Kinnison, D. E.: Tropospheric ozone decrease due  
811 to the Mount Pinatubo eruption: Reduced stratospheric influx, *Geophys Res Lett*, 40, 5553-  
812 5558, 10.1002/2013GL056563, 2013.

813 Tang, Q., Prather, M. J., Hsu, J. O., Ruiz, D. J., Cameron, P. J. S., Xie, S. C., and Golaz, J. C.:  
814 Evaluation of the interactive stratospheric ozone (O3v2) module in the E3SM version 1  
815 Earth system model, *Geosci Model Dev*, 14, 1219-1236, 10.5194/gmd-14-1219-2021, 2021.

816 Thompson, R. L., Patra, P. K., Ishijima, K., Saikawa, E., Corazza, M., Karstens, U., Wilson, C.,  
817 Bergamaschi, P., Dlugokencky, E., Sweeney, C., Prinn, R. G., Weiss, R. F., O'Doherty, S.,  
818 Fraser, P. J., Steele, L. P., Krummel, P. B., Saunio, M., Chipperfield, M., and Bousquet, P.:  
819 TransCom N2O model inter-comparison - Part 1: Assessing the influence of transport and  
820 surface fluxes on tropospheric N2O variability, *Atmos Chem Phys*, 14, 4349-4368, DOI  
821 10.5194/acp-14-4349-2014, 2014.

822 Tian, H. Q., Xu, R. T., Canadell, J. G., Thompson, R. L., Winiwarter, W., Suntharalingam, P.,  
823 Davidson, E. A., Ciais, P., Jackson, R. B., Janssens-Maenhout, G., Prather, M. J., Regnier,  
824 P., Pan, N. Q., Pan, S. F., Peters, G. P., Shi, H., Tubiello, F. N., Zaehle, S., Zhou, F., Arne,  
825 A., Battaglia, G., Berthet, S., Bopp, L., Bouwman, A. F., Buitenhuis, E. T., Chang, J. F.,  
826 Chipperfield, M. P., Dangal, S. R. S., Dlugokencky, E., Elkins, J. W., Eyre, B. D., Fu, B. J.,  
827 Hall, B., Ito, A., Joos, F., Krummel, P. B., Landolfi, A., Laruelle, G. G., Lauerwald, R., Li,  
828 W., Lienert, S., Maavara, T., MacLeod, M., Millet, D. B., Olin, S., Patra, P. K., Prinn, R. G.,  
829 Raymond, P. A., Ruiz, D. J., van der Werf, G. R., Vuichard, N., Wang, J. J., Weiss, R. F.,  
830 Wells, K. C., Wilson, C., Yang, J., and Yao, Y. Z.: A comprehensive quantification of  
831 global nitrous oxide sources and sinks, *Nature*, 586, 248-252, 10.1038/s41586-020-2780-0,  
832 2020.

833 Tokarska, K. B., Stolpe, M. B., Sippel, S., Fischer, E. M., Smith, C. J., Lehner, F., and Knutti,  
834 R.: Past warming trend constrains future warming in CMIP6 models, *Sci Adv*, 6, ARTN  
835 eaaz9549, 10.1126/sciadv.aaz9549, 2020.

836 Tung, K. K., and Yang, H.: Global QBO in Circulation and Ozone 1. Reexamination of  
837 Observational Evidence, *J Atmos Sci*, 51, 2699-2707, Doi 10.1175/1520-  
838 0469(1994)051<2699:Gqicao>2.0.Co;2, 1994b.

839 Tung, K. K., and Yang, H.: Global QBO in Circulation and Ozone 2. A Simple Mechanistic  
840 Model, *J Atmos Sci*, 51, 2708-2721, 10.1175/1520-0469(1994)051<2708:Gqicao>2.0.Co;2,  
841 1994a.

842 Williams, R. S., Hegglin, M. I., Kerridge, B. J., Jockel, P., Latter, B. G., and Plummer, D. A.:  
843 Characterising the seasonal and geographical variability in tropospheric ozone, stratospheric  
844 influence and recent changes, *Atmos Chem Phys*, 19, 3589-3620, 10.5194/acp-19-3589-  
845 2019, 2019.

846 WMO: Scientific Assessment of Ozone Depletion: 2018, Global Ozone Research and  
847 Monitoring Project—Report No. 58, World Meteorological Organization, Geneva,  
848 Switzerland, 588 pp., 2018.

849 Yang, H., Chen, G., Tang, Q., and Hess, P.: Quantifying isentropic stratosphere-troposphere  
850 exchange of ozone, *J Geophys Res-Atmos*, 121, 3372-3387, 10.1002/2015JD024180, 2016.

851 Young, P. J., Archibald, A. T., Bowman, K. W., Lamarque, J. F., Naik, V., Stevenson, D. S.,  
852 Tilmes, S., Voulgarakis, A., Wild, O., Bergmann, D., Cameron-Smith, P., Cionni, I., Collins,  
853 W. J., Dalsoren, S. B., Doherty, R. M., Eyring, V., Faluvegi, G., Horowitz, L. W., Josse, B.,  
854 Lee, Y. H., MacKenzie, I. A., Nagashima, T., Plummer, D. A., Righi, M., Rumbold, S. T.,  
855 Skeie, R. B., Shindell, D. T., Strode, S. A., Sudo, K., Szopa, S., and Zeng, G.: Pre-industrial  
856 to end 21st century projections of tropospheric ozone from the Atmospheric Chemistry and  
857 Climate Model Intercomparison Project (ACCMIP), *Atmos Chem Phys*, 13, 2063-2090,  
858 DOI 10.5194/acp-13-2063-2013, 2013.

859 Young, P. J., Naik, V., Fiore, A. M., Gaudel, A., Guo, J., Lin, M. Y., Neu, J. L., Parrish, D. D.,  
860 Rieder, H. E., Schnell, J. L., Tilmes, S., Wild, O., Zhang, L., Ziemke, J., Brandt, J., Delcloo,  
861 A., Doherty, R. M., Geels, C., Hegglin, M. I., Hu, L., Im, U., Kumar, R., Luhar, A., Murray,  
862 L., Plummer, D., Rodriguez, J., Saiz-Lopez, A., Schultz, M. G., Woodhouse, M. T., and  
863 Zeng, G.: Tropospheric Ozone Assessment Report: Assessment of global-scale model  
864 performance for global and regional ozone distributions, variability, and trends, *Elementa-*  
865 *Science of the Anthropocene*, 6, 2018.

866 Zeng, G., Morgenstern, O., Braesicke, P., and Pyle, J. A.: Impact of stratospheric ozone recovery  
867 on tropospheric ozone and its budget, *Geophys. Res. Lett.*, 37, L09805,  
868 10.1029/2010gl042812, 2010.

869 Ziemke, J. R., Oman, L. D., Strode, S. A., Douglass, A. R., Olsen, M. A., McPeters, R. D.,  
870 Bhartia, P. K., Froidevaux, L., Labow, G. J., Witte, J. C., Thompson, A. M., Haffner, D. P.,  
871 Kramarova, N. A., Frith, S. M., Huang, L. K., Jaross, G. R., Seftor, C. J., Deland, M. T., and  
872 Taylor, S. L.: Trends in global tropospheric ozone inferred from a composite record of  
873 TOMS/OMI/MLS/OMPS satellite measurements and the MERRA-2 GMI simulation,  
874 *Atmos Chem Phys*, 19, 3257-3269, 10.5194/acp-19-3257-2019, 2019.

875  
876